Energy Efficient Resource Allocation for Multinumerology Enabled Hybrid Services in B5G Wireless Mobile Networks

Li-Hsiang Shen, *Member, IEEE*, Pei-Ying Wu, and Kai-Ten Feng, *Senior Member, IEEE*

***Abstract*— Multi-numerology (MN) providing a flexible transmission frame structure has attracted a considerable attention for supporting abundant services for beyond fifth-generation (B5G) networks. However, mobility induces severe performance degradation under different numerologies including temporal and spectral fluctuation, which is not well-investigated in existing literature. We have conceived an MN-enabled energy efficiency (EE) problem aiming for alleviating mobility- and MN-induced interferences through moderate power and sub-carrier assignment, while considering quality-of-service (QoS) and latency requirements for different services. We propose a multi-numerology based power and resource block allocation (MNPRA) scheme considering time-/frequency-division (TD/MD) based MN leveraging temporal and spectral features among numerologies. The original non-solvable problem is theoretically transformed into a convex one by employing Dinkelbach process, Taylor approximation and difference of two concave functions (D.C.). Convergence of proposed MNPRA scheme is analyzed and verified by simulations. In simulation results, we have evaluated MNPRA under different service demands, user velocities and MN types. Our proposed scheme outperforms the conventional single-numerology framing and existing methods in open literature, which results in performances of higher EE as well as of lower throughput/delay outage probability.**

***Index Terms*— B5G, multi-numerology, enhanced mobile broadband (eMBB), ultra-reliable and low latency communications (URLLC), resource allocation, energy efficiency, user mobility.**

I. Introduction

IN RECENT decades, there emerge diverse service types and increasing traffic demands for beyond fifth-generation (B5G) wireless networks such as latency-aware vehicular communications, reliability demands for smart applications, massive connectivity for internet-of-everything, and throughput-oriented ultra-high definition [1]. As elaborated in 5G specification, the 3rd generation partnership project (3GPP) has classified abundant scenarios into three primary use cases including enhanced mobile broadband (eMBB), massive machine-type communications (mMTC), and ultra-reliable and low-latency communications (URLLC) [2]. Furthermore, B5G promises unprecedented performance enhancement for various applications of further-eMBB (FeMBB), extremely-URLLC (EURLLC) and ultra-mMTC (umMTC) [3] providing over ten times spectrum efficiency and one tenth latency compared to existing 5G communications.

Accordingly, single-numerology (SN) system, i.e., a single transmission frame applied for a service type is utilized in traditional networks, which is potentially nonresilient due to various service demands. As a prospect mechanism specified in 5G new radio (5G-NR), it introduces multi-numerology (MN) that allows flexible transmission framing to supply ample service types [4]. The term *numerology* refers to as the parameterization of physical transmit waveform [5]. Different numerology types possess different sub-carrier spacings (SCSs) and symbol durations in spectral and temporal domains of resource blocks (RBs). For the latency-critical requirement, it is intuitive to assign RBs in a numerology type with larger SCS and shorter symbol duration, and vice versa for rate-oriented applications [6], which however induces potential tradeoff among numerologies. For instance, short symbol duration with low-latency provokes higher control overhead and lower signal gain [7], [8], whereas a larger SCS with high-rate declines the resource utilization. In papers [9], [10], [11], [12], they consider power-RB allocation under conventional SN mechanism while guaranteeing quality-of-service (QoS) and latency restriction. Moreover, papers [13], [14], [15] support high-speed applications under single-numerology based scheduling. The work in [13] has conducted a velocity-adaptive power allocation considering the QoS and fairness among users, whilst papers [14], [15] aim at maximizing system rate considering channel conditions of both mobile and static users. The authors of [15] optimize energy efficiency (EE) for versatile users under high-speed environments. However, system rate-latency performance cannot be simultaneously taken into account under plentiful types of services, which is confined by unavailability of different numerologies as in [9], [10], [13], [14], and [15].

To conquer the dilemma of SN mechanism mentioned above, allocation of numerologies for different services becomes substantially important as investigated in [16], [17],

Manuscript received 1 March 2022; revised 16 July 2022; accepted 7 September 2022. Date of publication 21 September 2022; date of current version 10 March 2023. This work was supported in part by the Ministry of Science and Technology (MoST) under Grant 110-2221-E-A49-041-MY3, Grant 110-2221-E-A49-027-MY2, Grant 111-2218-E-A49-024, and Grant 111-3114-E-A49-001; in part by the Science, Technology, Engineering and Math (STEM) Project; in part by the National Defense Science and Technology Academic Collaborative Research Project in 2022; and in part by the Higher Education Sprout Project of the National Yang Ming Chiao Tung University and Ministry of Education (MoE), Taiwan. The associate editor coordinating the review of this article and approving it for publication was L. Duan. *(Corresponding author: Kai-Ten Feng.)*

The authors are with the Department of Electronics and Electrical Engineering, National Yang Ming Chiao Tung University (NYCU), Hsinchu 300093, Taiwan (e-mail: gp3xu4vu6.cm04g@nctu.edu.tw; iampeggy.cm08g@nctu.edu.tw; ktfeng@nycu.edu.tw).

Color versions of one or more figures in this article are available at https://doi.org/10.1109/TWC.2022.3206589.

Digital Object Identifier 10.1109/TWC.2022.3206589

[18], [19], [20], and [21]. The authors of [16] have addressed a scheduling problem by selecting different numerologies for each user with diversified service demands. The paper [17] has issued a delay-aware problem of URLLC users while maximizing the overall system EE. A joint power and RB allocation problem is investigated in [18] whose target is to minimize downlink power consumption under a heterogeneous network. However, the papers of [16], [17], [18] do not consider the inter-numerology interference (INI) caused by the overlapped numerologies [19], [20]. As analyzed in [19] and [20], INI cannot be neglected due to its serious interfered power induced by non-orthogonal transmission frames. Note that [19], [20] have analyzed INI and designed mitigation mechanism on waveforms from the physical layer perspective under the fixed numerology configuration. To mitigate INI, the work in [21] has employed multiplexing in time-domain based numerology rather than in frequency-domain, i.e., a single numerology type is configured at each timeslot to fulfill specific service requirement. Nonetheless, it has potentially lower flexibility compared to the system using frequency-domain based numerology in [16], [17] and [18]. Therefore, papers [5], [22], [23] have studied the architecture of multi-numerology with consideration of INI. The authors of [22] have designed a heuristic method to minimize INI by adjusting the power difference of RBs. While, the works of [5], [23] assign appropriate power to maximize INI-aware throughput. Furthermore, it is noticed that current INI-related works consider fixed numerology bandwidth ratio (NBR) among different numerologies, i.e., the number of RBs utilized by a specific numerology is predefined [19]. Nevertheless, INI can be possibly leveraged according to different utilized bandwidths compromising service requirements. Different number of available RBs for the respective numerologies should be jointly considered with power and RB allocation to mitigate total INI, which is not considered in most of existing papers.

Moreover, high mobility wireless networks such as vehicle, drone and high-speed railway communications have attracted compelling attention [24], [25], [26]. Accordingly, the next-generation wireless network is prospected to flexibly accommodate mobility-aware channels. Under high-speed scenario, it has to overcome the performance degradation induced by inter-carrier interference (ICI) from Doppler spread effect [27]. While, it also requires to conquer inter-symbol interference (ISI) caused by delay spread [27]. As for multi-numerology, the system becomes more robust to interference where flexible RB with large SCS can reduce ICI, whereas small SCS can be applied against the ISI effect. Additionally, latency limitation is not studied in papers of [5], [13], [14], [15], [21], [22], which is specifically critical in most of high-speed wireless networks. The papers [4], [28], [29] have exploited the scalable numerology structure to meet the requirement of multi-services. The authors of [28] apply convex optimization to solve the RB allocation problem for a MN system with random ISI and ICI effects. In paper [29], the authors have formulated a two-dimensional (2D) resource allocation problem, i.e., time and frequency domains aiming at maximizing the achievable rate while restricting latency-aware demands. The paper [4] resolves a throughput maximization problem considering latency demands, which exhibits the random INI, ISI and ICI impacts on MN. However, actual channel is not well modeled but utilizing a random variance to characterize interferences. Furthermore, NBR and appropriate power assignment are not discussed which potentially generate higher interference resulting in a lower throughput and EE performance.

Note that RB allocation represents time-frequency domain constituted resource grids (RGs), whilst NBR allocation indicates total utilized bandwidth ratios of different numerologies. However, based on the investigation of state-of-the-art works, they consider simple models of the MN system without practical terms of interferences. Moreover, most of existing works target on the rate optimization, which however may waste power resource to satisfy the demands. We also extend from our previous works in [11], [12] and [23], which are focused on SN-based resource allocation for single and multi-services as well as for the fixed MN scenario, respectively. To achieve higher EE, conceiving a flexible MN mechanism becomes compellingly imperative under comprehensive resource utilizations and interference considerations for supporting different service requirements. Motivated by existing works, we aim at optimizing EE performance with joint power, RB and NBR assignments under interference factors of INI, ISI and ICI in a mobility-aware MN-based hybrid services. The main contributions of this work are summarized as follows.

- We have studied the mobility-aware MN network supporting hybrid services of eMBB and URLLC users. Moreover, the proposed signal model reflects all interference factors of ICI, ISI and INI caused by Doppler spread, delay spread and inter-numerology influence. We jointly allocate power, RBs and bandwidth ratio between numerologies to maximize the system EE while guaranteeing QoS and latency requirement, which are not jointly considered in existing literature.
- We have proposed a multi-numerology based power and resource block allocation (MNPRA) scheme to solve the EE maximization problem. The original fractional objective is transformed into a subtractive form by the Dinkelbach method. Based on the auxiliary integer relaxation, it converts the discrete variables into continuous ones. Moreover, benefited by approximation from difference of two concave functions (D.C.), the NP-hard problem becomes a convex one, which is followed by the convergence and complexity analysis of the proposed MNPRA scheme.
- We consider two types of mobility-aware MN including time-division (TD) and frequency-division (FD) leveraging temporal and spectral widths among numerologies. In TD-MN, it potentially mitigates INI by assigning a single numerology type at a single timeslot, whereas NBR is optimized in FD-MN containing multiple numerologies within a timeslot to compromise induced interferences and service constraints.
- Simulation results reveal the nature of ISI, ICI and INI under different configurations. While, MN related parameters are evaluated under various QoS, latency constraints, velocity, and scenarios with different numbers

of eMBB/URLLC users. As a benefit of flexible mobility-aware MN network, the proposed MNPRA algorithm outperforms the existing benchmarks in open literature in terms of the lowest power consumption and the highest throughput/EE performance.

The rest of this article is organized as follows. In Section II, we present the system model and problem formulation of considered MN system. The proposed MNPRA scheme is introduced in Section III. Analysis of MNPRA, including problem transformation and approximation is demonstrated in Section III-C. Section IV evaluates the results and benchmark comparisons, whilst the conclusion is drawn in Section V.

II. System Model and Problem Formulation

A. System Model

We consider a downlink orthogonal frequency division multiplexing (OFDM) based base station (BS) serving two different types of $\mathcal{N} = \{1, 2, \ldots, N\}$ users with eMBB $\mathcal{N}_e = \{1, 2, \ldots, N_e\}$ and URLLC $\mathcal{N}_u = \{1, 2, \ldots, N_u\}$ users. We define numerology set of $\mathcal{I} = \{1, 2, \ldots, I\}$, where two numerologies[1] are considered as $I = 2$ with each having SCS of Δf_i and corresponding symbol time duration of T_i. Based on [30], $\Delta f_i \cdot T_i$ is a constant for all i to guarantee equivalent data amount. We define $\Delta f_i = 2^{s_i} \times 15$ (kHz) and s_i as available SCS levels specified in the new radio (NR) protocol [30]. Note that we consider $\Delta f_1 < \Delta f_2$ and thus $T_1 > T_2$ without loss of generality. We also denote the system bandwidth as BW and total frame duration as T_{total}.

1) Two-Dimensional (2D) Frame Structure: To support multiple service requirements by utilizing flexible numerologies, we introduce a 2D frame structure containing different size of resource blocks (RBs). As illustrated in Fig. 1, we construct a resource grid (RG) via the greatest common divisor, i.e., the RG is spanned by T_2 in time-domain and by Δf_1 in frequency-domain. The total bandwidth is further divided into sub-carrier sets of numerology-1 as $\mathcal{F}_1 = \{1, 2, \ldots, F_1\}$ and of numerology-2 as $\mathcal{F}_2 = \{1, 2, \ldots, F_2\}$. Note that several RGs can generate an RB. Therefore, two types of RBs are introduced in our system with one having a larger SCS while the other possessing longer symbol duration. It can be observed that it becomes difficult to align symbols in an MN system. Accordingly, we partition all RBs into L RB groups (RBG) by aligning T_1 as the least common multiplier of symbol duration [31], and we denote the RBG set as $\mathcal{L} = \{1, 2, \ldots, L\}$, which is shown on the left-hand side of Fig. 1. Moreover, RBs within an RBG are configured in the order from $f = 1$ to $f = F_1$ and from left $t = 1$ to right $t = T$. The frequency indexes of two numerologies are different due to distinct SCSs. We denote the RB set in an RBG as

[1]Here, it would be observable by considering 2 numerologies to know its nature of interferences and see how they impact on the system performance. Note that the designed model can be extended to more than 3 numerologies with more complicate modeling. The key concept is the calculation of indexing via greatest common divisor (gcd) among different numerologies. For general case extension, we can adjust the ordering equations of (1)–(3) with $i \geq 3$, as well as the INI model in (6) and (7) with additional summation index of $i \in \mathcal{I}$.

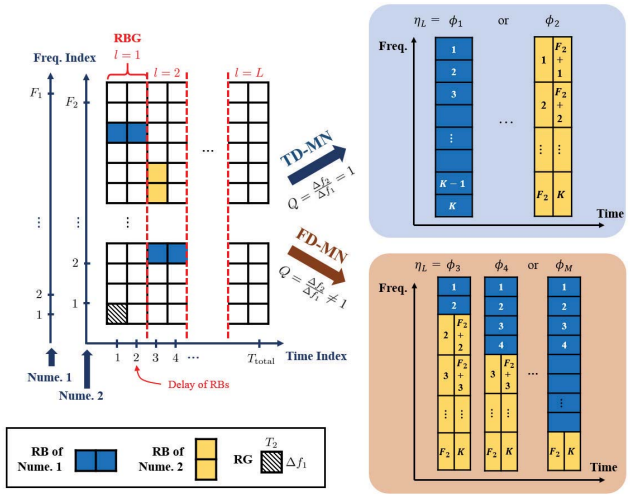

Fig. 1. Structure of numerology types in terms of establishment of RBs in time-/frequency-domains.

$\mathcal{K} = \{1, 2, \ldots, K\}$. Note that as exemplified in two-numerologies in Fig. 1, indexes for numerology-2 do not always start from 1 which are replaced by indexes of numerology-1. Therefore, the k-th RB with numerology i in the l-th RBG is indexed by the tuple of $\{(k \bmod F_i), \Theta(l, i, k)\}$, where $(k \bmod F_i)$ is frequency-domain index with module operation mod, whilst $\Theta(l, i, k)$ denotes the delay in time-domain given by

$$\Theta(l,i,k) = \begin{cases} \dfrac{\Delta f_2}{\Delta f_1} \cdot l, & i = 1, \\ \dfrac{\Delta f_2}{\Delta f_1} \cdot (l-1) + \left\lceil \dfrac{k}{F_2} \right\rceil, & i = 2, \end{cases} \tag{1}$$

where $\lceil \cdot \rceil$ is the ceiling function, which means that it may possess lower delay in numerology-2 when $i = 2$ as shown in Fig. 1. Note that the unit of delay (1) is in the unit of RBG slot with the similar definition as in [16], [17], and [4]. For example, we have delay in the unit of $\Theta(1, 1, k) = 2$ RG-slots and $\Theta(2, 1, k) = 4$ slots for $l = 1$ and $l = 2$ when $i = 1$, respectively. However, when $i = 2$, $\Theta(1, 2, k) = 1, \forall k \in \{1, 2, \ldots, F_2\}$ and $\Theta(1, 2, k) = 2, \forall k \in \{F_2 + 1, F_2 + 2, \ldots, K\}$ are RG-slot delay for RBs using numerology-2 in $l = 1$ RBG, whilst we can calculate the following in similar manner as $\Theta(2, 2, k) = 3, \forall k \in \{1, 2, \ldots, F_2\}$ and $\Theta(2, 2, k) = 4, \forall k \in \{F_2 + 1, F_2 + 2, \ldots, K\}$ in $l = 2$.

2) TD-/FD-MN: We consider two kinds of MN including TD and FD based configurations. TD-MN allows a single numerology type within a single time duration, and different services are multiplexed in time-domain. While, FD-MN allows co-existence of numerologies at each time instant, i.e., partial RBs are for numerology-1 and the others are for numerology-2. It becomes a compelling trade-off leveraging INI alleviation under TD-MN and high flexibility of FD-MN for throughput-oriented or latency-aware demands [32]. As depicted in Fig. 1, we define $Q = \frac{\Delta f_2}{\Delta f_1}$ as the ratio of two SCSs from the selected numerologies. Note that $Q = 1$ indicates that only one numerology is selected which

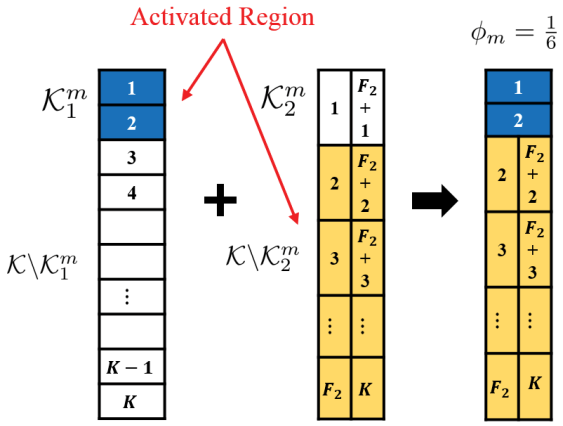

Fig. 2. Example for activated RBs with two numerologies with $\phi_m = \frac{1}{6}$, $F_1 = 12$ and $F_2 = 6$. Note that $\mathcal{K}_1^m$ has numerology-1's index set $\{1, 2\}$, whereas $\mathcal{K}_2^m$ has numerology-2's index set $\{1, F_2 + 1\}$. The activation RBs are shown in blue and yellow for numerology-1 and numerology-2, respectively, which follows the condition of $k \in \mathcal{K}_1^m$ when $i = 1$ and $k \in \mathcal{K}\backslash\mathcal{K}_2^m$ when $i = 2$.

is deemed to be TD-MN, whereas it is FD-MN when $Q \neq 1$. Therefore, we can have different flexible configurations of MN with various NBR values indicating how many bandwidths are occupied by a certain numerology type. Due to countable RBs, all possible NBR values can be acquired as

$$\phi_m = \begin{cases} \dfrac{j_1}{F_2}, & \text{where } j_1 \in \{0, F_2\}, \forall j_1 \in \mathbb{Z}, \text{ if } Q = 1, \\ \dfrac{j_2}{F_2}, & \text{where } 1 \leq j_2 \leq F_2 - 1, \forall j_2 \in \mathbb{Z}, \text{ if } Q \neq 1. \end{cases} \tag{2}$$

Note that M is the total number of possible NBR values with the total set of $\mathcal{M} = \{1, 2, \ldots, M\}$. Let us take $F_2 = 6$ for example, we can derive $\phi_m \in \{0, \frac{1}{6}, \frac{2}{6}, \ldots, 1\}$ with $M = 8$. As exemplified on the right-hand side of Fig. 1 as well as in Fig. 2, $\phi_1 = 0$ and $\phi_2 = 1$ stands for TD-MN with SCSs Δf_1 and Δf_2, respectively. As for FD-MN, $\phi_3 = \frac{1}{6}$ indicates two RBs for SCS Δf_1 and the remains for SCS Δf_2. To adjust NBR, we consider a binary indicator $\alpha_{l,m} \in \{0, 1\}$ which $\alpha_{l,m} = 1$ implies that we select ϕ_m as the NBR in the l-th RBG. We notice that in each RBG we can only choose a single ϕ_m, i.e., $\sum_{m\in\mathcal{M}} \alpha_{l,m} = 1, \forall l \in \mathcal{L}$. Accordingly, based on $\alpha_{l,m}$ and ϕ_m, we can obtain $0 \leq \eta_l = \sum_{m\in\mathcal{M}} \alpha_{l,m}\phi_m \leq 1$ as the candidate NBR value in the l-th RBG, that is, numerology-1 will occupy a ratio of η_l of bandwidth, whilst numerology-2 takes the rest of a ratio of $(1 - \eta_l)$. Therefore, deciding a discrete policy of η_l is equivalent to determining the indicator $\alpha_{l,m}$. We denote $\omega_{i,k}^m$ as the activation indicator[2] to represent whether the k-th RB under numerology i is applying the m-th NBR value ϕ_m, which can be derived by

$$\omega_{i,k}^m = \begin{cases} 1, & k \in \mathcal{K}_1^m, \ i = 1, \text{ or } \ k \in \mathcal{K}\backslash\mathcal{K}_2^m, \ i = 2, \\ 0, & k \in \mathcal{K}\backslash\mathcal{K}_1^m, \ i = 1, \text{ or } \ k \in \mathcal{K}_2^m, \ i = 2, \end{cases} \tag{3}$$

[2]Note that we could define a compound variable combining both $\alpha_{l,m}$ and $\omega_{i,k}^m$. However, we keep $\alpha_{l,m}$ simple and neat and let the non-solvable expression emerge in $\omega_{i,k}^m$ in the interference model, which benefits the problem transformation and derivation by depending only on the binary policy of $\alpha_{l,m}$.

where $\mathcal{K}_1^m = \{1, 2, \ldots, \phi_m F_1\}$ and $\mathcal{K}_2^m = \{(q-1)F_2 + 1, (q-1)F_2 + 2, \ldots, (q-1)F_2 + \phi_m F_2 \mid \forall q \in \mathbb{Z}, 1 \leq q \leq \frac{\Delta f_2}{\Delta f_1}\}$. In Fig. 2, we take $\phi_m = \frac{1}{6}$, $F_1 = 12$ and $F_2 = 6$ for example with its outcome of $\mathcal{K}_1^m$'s index set of $\{1, 2\}$ and $\mathcal{K}_2^m$'s index set of $\{1, F_2 + 1\}$. We can know from Fig. 2 that top two RBs are occupied by numerology-1 with $\mathcal{K}_1^m$'s and the remaining ones are allocated to $\mathcal{K}_2^m$, which follows the activation condition in the first criterion of (3). According to the above definition, $\alpha_{l,m}\omega_{i,k}^m = 1$ indicates that we firstly select the m-th NBR value ϕ_m in the l-th sub-RG as $\alpha_{l,m} = 1$, whereas the k-th RB of numerology i in RBG l is available to be allocated to users as $\omega_{i,k}^m = 1$.

3) Signal Model: We define $P_{i,k}^{n,l}$ as the power allocated to the n-th user on the k-th RB of numerology i in RBG l. The channel loss is denoted as $h_{i,k}^{n,l} = \beta_{i,k}^{n,l} d_n^{-\varrho}$, where $\beta_{i,k}^{n,l}$ is Rayleigh small-scale fading and $d_n^{-\varrho}$ indicates the distance based large-scale fading with distance d_n and pathloss exponent ϱ. The RB assignment indicator is defined as $\rho_{i,k}^{n,l} \in \{0, 1\}$. Note that $\rho_{i,k}^{n,l} = 1$ means that the k-th RB in numerology i of RBG l is allocated to user n, and vice versa for $\rho_{i,k}^{n,l} = 0$.

Owing to different mobility-aware channel conditions and the non-orthogonality induced from MN, interferences from ICI, ISI, and INI should be jointly alleviated and modelled in the problem, which are not considered in most of existing open literature. Inspired by Jakes' power spectral density model, we can obtain the ICI function [33] for the k-th RB in RBG l under numerology i as

$$\begin{aligned} ICI_{i,k}^l &= \frac{1}{2\Delta {f_i}^2} \sum_{n=1}^{N} \sum_{\substack{f'=1 \\ f' \neq (k \bmod F_i)}}^{F_i} \frac{1}{\left[f' - (k \bmod F_i)\right]^2} \left(\frac{f_c}{c} v_n\right)^2 \\ &\quad \cdot P_{i,f''}^{n,l} \rho_{i,f''}^{n,l} \sum_{m\in\mathcal{M}} \alpha_{l,m}\omega_{i,f''}^m, \end{aligned} \tag{4}$$

where v_n, f_c and c are velocity of user n, operating carrier frequency and the speed of light, respectively. The subscript $f'' = F_i\left(\left\lceil \frac{k}{F_i} \right\rceil - 1\right) + f'$ is the RB index for sub-carrier f' under numerology i. It can be seen that higher velocity and frequency bands will intrinsically provoke large ICI, which can be compromised by assigning proper power $P_{i,f''}^{n,l}$, RB policy $\rho_{i,f''}^{n,l}$ and NBR policy $\alpha_{l,m}$. Based on paper [34], the ISI function in an MN system can be derived as

$$\begin{aligned} ISI_{i,k}^{n,l} &= P_{i,k}^{n,l} \rho_{i,k}^{n,l} \left(\sum_{m\in\mathcal{M}} \alpha_{l,m}\omega_{i,k}^m\right) \Delta f_i \\ &\quad \cdot \int_0^{\xi_{\text{RMS}} - \frac{\gamma}{\Delta f_i}} \int_{\frac{\gamma}{\Delta f_i} + t}^{\xi_{\text{RMS}}} \Xi(\xi)\, d\xi dt, \end{aligned} \tag{5}$$

where ξ_{RMS} is the root mean square (RMS) signal delay spread, γ is the cyclic prefix ratio in OFDM, and $\Xi(\xi)$ is the function of the channel power delay profile which can be asymptotically approximated as an exponential distribution based on [35]. According to [36], there arise asymmetric interference impacts from two different numerology types which should be also taken into account in INI. We can write out the MN-based

INI function as the received interference of numerology-2 from numerology-1 as

$$INI^{l}_{1\to 2,k} = \sum_{n=1}^{N}\sum_{f'=1}^{F_1}\frac{P^{n,l}_{1,f'}\rho^{n,l}_{1,f'}}{F_1F_2}\sum_{m\in\mathcal{M}}\alpha_{l,m}\omega^{m}_{1,f'}\delta_{1\to 2,m}, \tag{6}$$

and interference of numerology-1 from numerology-2 as

$$\begin{aligned} INI^{l}_{2\to 1,k} = &\sum_{n=1}^{N}\sum_{f'=1}^{F_2}\frac{P^{n,l}_{2,f'}\rho^{n,l}_{2,f'}}{F_1F_2}\sum_{m\in\mathcal{M}}\alpha_{l,m}\omega^{m}_{2,f'}\delta^{(1)}_{2\to 1,m} \\ &+\sum_{n=1}^{N}\sum_{f'=1}^{F_2}\sum_{q=1}^{Q-1}\frac{P^{n,l}_{2,F_2q+f'}\rho^{n,l}_{2,F_2q+f'}}{F_1F_2} \\ &\times\sum_{m\in\mathcal{M}}\alpha_{l,m}\omega^{m}_{2,F_2q+f'}\delta^{(2)}_{2\to 1,m}, \end{aligned} \tag{7}$$

where the pertinent parameters in INI functions are expressed as (8)–(10), shown at the bottom of the next page. We can observe from INI models that when $Q = 1$, the values of sine functions become zero in numerators of both (6) and (7), i.e., no interference $INI^{l}_{i'\to i,k} = 0$ is induced due to orthogonality property in either TD-MN or single-numerology system.

Considering all interference factors as defined above, the received signal-to-interference-plus-noise ratio (SINR) of user n on RB k in RBG l under numerology i is formulated as

$$\Gamma^{n,l}_{i,k} = \frac{P^{n,l}_{i,k}\left|h^{n,l}_{i,k}\right|^2\rho^{n,l}_{i,k}\cdot\sum_{m\in\mathcal{M}}\alpha_{l,m}\omega^{m}_{i,k}}{ICI^{l}_{i,k}+ISI^{n,l}_{i,k}+INI^{l}_{i'\to i,k}+N_0\cdot\Delta f_i}, \tag{11}$$

where $INI^{l}_{i'\to i,k}$ is INI from other numerologies with $i'\neq i$, and N_0 is the noise power spectral density. By determining the policy set of power $\boldsymbol{P} = \{P^{n,l}_{i,k}|\forall n\in\mathcal{N}, l\in\mathcal{L}, i\in\mathcal{I}, k\in\mathcal{K}\}$, RB assignment $\boldsymbol{\rho} = \{\rho^{n,l}_{i,k}|\forall n\in\mathcal{N}, l\in\mathcal{L}, i\in\mathcal{I}, k\in\mathcal{K}\}$ and NBR indicator $\boldsymbol{\alpha} = \{\alpha_{l,m}|\forall l\in\mathcal{L}, m\in\mathcal{M}\}$, the throughput of user n can thus be derived by

$$R^{n}(\boldsymbol{P},\boldsymbol{\rho},\boldsymbol{\alpha}) = \sum_{l\in\mathcal{L}}\sum_{i\in\mathcal{I}}\sum_{k\in\mathcal{K}}T_i\cdot\Delta f_i\cdot\log_2\left(1+\Gamma^{n,l}_{i,k}\right). \tag{12}$$

Note that total transmit data amount is considered for both eMBB and URLLC users in (12) by leveraging the Shannon throughput as well as time duration, which is different from the existing works of [17] and [4] considering only Shannon throughput. The power consumption of user n in the l-th RBG is expressed as

$$P^{n,l}(\boldsymbol{P},\boldsymbol{\rho},\boldsymbol{\alpha}) = \sum_{i\in\mathcal{I}}\sum_{k\in\mathcal{K}}\frac{T_i}{T_1}\left(\eta_{\text{PA}}P^{n,l}_{i,k}\rho^{n,l}_{i,k}\sum_{m\in\mathcal{M}}\alpha_{l,m}\omega^{m}_{i,k}\right) + P_{\text{circuit}}, \tag{13}$$

where η_{PA} is the power amplifier efficiency, and P_{circuit} is the constant circuit power consumption averaged over each RBG. To characterize the joint performance of throughput and power, we are able to acquire the system EE according to (12) and (13) as

$$\Lambda(\boldsymbol{P},\boldsymbol{\rho},\boldsymbol{\alpha}) = \frac{\sum_{n\in\mathcal{N}}R^{n}(\boldsymbol{P},\boldsymbol{\rho},\boldsymbol{\alpha})}{\sum_{n\in\mathcal{N}}\sum_{l\in\mathcal{L}}P^{n,l}(\boldsymbol{P},\boldsymbol{\rho},\boldsymbol{\alpha})}. \tag{14}$$

B. Problem Formulation

For the optimization problem in a mobility-aware MN system, we aim at maximizing the system EE by optimally determining the policy of power, RB and NBR assignments constrained by available resources and service requirements, which is formulated as (15a)–(15k), shown at the bottom of the next page. Constraints (15b), (15c) guarantee the QoS requirements of $R^{e}_{\min}$ and $R^{u}_{\min}$ for throughput-oriented eMBB and latency-aware URLLC users. Note that without loss of generality, $R^{e}_{\min}$ has a much higher value than that of $R^{u}_{\min}$. Moreover, constraints (15d), (15e) confine the latency restrictions of both eMBB and URLLC services with τ_e and τ_u, respectively. Similarly, more stringent service of smaller τ_u for URLLC should be guaranteed, i.e., in general we have $\tau_u < \tau_e$. The limitation of per-RB transmit power and total BS power are respectively defined as $P_{\max}$ in constraint (15f) and as $P^{\text{tot}}_{\max}$ in (15g). Note that (15f) confines per-RB power to prevent greedy assignment consuming full power from a certain RB leading to inappropriate candidate solution set. In (15i) and (15h), we represent the discrete policy of RB allocation $\rho^{n,l}_{i,k}$ and NBR adjustment $\alpha_{l,m}$. Constraint (15j) implies that only one NBR value of ϕ_m can be selected in an RBG. While, constraint (15k) indicates that the activation of RB k in RBG l for numerology i is activated, that is, $\sum_{n\in\mathcal{N}}\rho^{n,l}_{i,k} = \sum_{m\in\mathcal{M}}\alpha_{l,m}\omega^{m}_{i,k} = 1$ means that the RB is activated and can be allocated to a single user, and vice versa. We can observe that the optimization problem $\mathcal{P}1$ in (15) is complex and non-solvable due to non-linearity and non-convexity properties owing to the fractional objective, the coupled discrete and continuous variables, and the non-concave throughput function, which is regarded as a non-convex mixed-integer non-linear problem (MINLP) and hence an NP-hard problem [37]. Therefore, we will transform the original problem into a solvable one by proposing the MNPRA scheme which is elaborated in the followings.

III. Proposed Multi-Numerology Based Power and Resource Block Allocation (MNPRA) Algorithm

A. Problem Transformation

To convert the considered complicated problem into a tractable one, we have to first tackle the fractional objective, coupled continuous and discrete variables and the non-convexity caused by interferences of ICI, ISI, and INI. In the followings, we will introduce some mathematical transformations and variable relaxing methods to handle these problems. The flowchart of problem transformation for proposed MNPRA algorithm is summarized in Fig. 3.

1) Transformation of Fractional Objective: Based on the fractional form in our objective function, we adopt the Dinkelbach method to transform a fractional function into a subtractive and linear expression [38]. We define $\mathcal{D}$ as the feasible set of policy in problem $\mathcal{P}1$ consisting of all possible constraints in (15b)–(15k). Therefore, under constrained set of $\mathcal{D}$, there exists an optimal EE λ^* which can be expressed as

$$\lambda^* = \max_{\{\boldsymbol{P},\boldsymbol{\rho},\boldsymbol{\alpha}\}\in\mathcal{D}}\Lambda(\boldsymbol{P},\boldsymbol{\rho},\boldsymbol{\alpha})$$

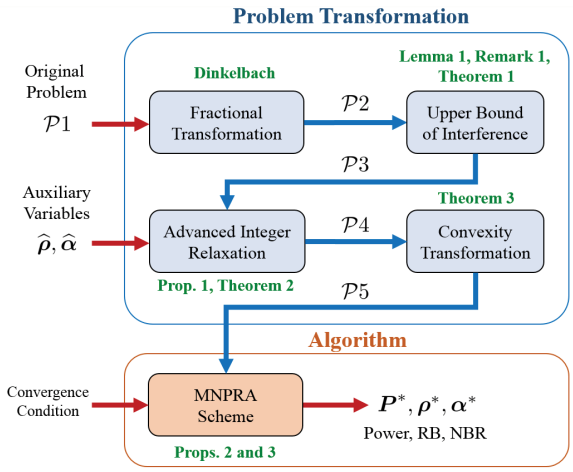

Fig. 3. The procedure of problem transformation for proposed MNPRA scheme.

$$= \frac{\sum_{n\in\mathcal{N}} R^n(\boldsymbol{P}^*,\boldsymbol{\rho}^*,\boldsymbol{\alpha}^*)}{\sum_{n\in\mathcal{N}}\sum_{l\in\mathcal{L}} P^{n,l}(\boldsymbol{P}^*,\boldsymbol{\rho}^*,\boldsymbol{\alpha}^*)}, \tag{16}$$

where the set of $\{\boldsymbol{P}^*,\boldsymbol{\rho}^*,\boldsymbol{\alpha}^*\}$ indicates the optimal allocation policy of power, RB assignment, and NBR adjustment, respectively. We can infer that the optimal EE in (16) is obtained if and only if the following problem holds

$$\begin{aligned}(\mathcal{P}2):\quad &\max_{\{\boldsymbol{P},\boldsymbol{\rho},\boldsymbol{\alpha}\}\in\mathcal{D}} \sum_{n\in\mathcal{N}} R^n(\boldsymbol{P},\boldsymbol{\rho},\boldsymbol{\alpha}) - \lambda^* \\ &\times \left(\sum_{n\in\mathcal{N}}\sum_{l\in\mathcal{L}} P^{n,l}(\boldsymbol{P},\boldsymbol{\rho},\boldsymbol{\alpha})\right) \qquad (17)\\ &= \sum_{n\in\mathcal{N}} R^n(\boldsymbol{P}^*,\boldsymbol{\rho}^*,\boldsymbol{\alpha}^*) - \lambda^* \\ &\times \left(\sum_{n\in\mathcal{N}}\sum_{l\in\mathcal{L}} P^{n,l}(\boldsymbol{P}^*,\boldsymbol{\rho}^*,\boldsymbol{\alpha}^*)\right) = 0. \qquad (18)\end{aligned}$$

Note that in $\mathcal{P}2$, the solution set of $\mathcal{D}$ exists as a non-empty feasible set when $\min\ R^n(P_{\max},\boldsymbol{\rho},\boldsymbol{\alpha}) \geq R^x_{\min}$, $\max\ \Theta(l,i,k)\rho^{n,l}_{i,k} \leq \tau_x$, and $\sum_{l\in\mathcal{L}}\sum_{i\in\mathcal{I}}\sum_{k\in\mathcal{K}}\rho^{n,l}_{i,k} \geq 1$, $\forall n\in\mathcal{N}_x, x\in\{e,u\}, l\in\mathcal{L}, i\in\mathcal{I}, k\in\mathcal{K}$. Such condition indicates that under the case at least one RB is assigned to each user with maximum power, we can acquire a feasible set by guaranteeing the worst throughput/latency being above/below the predefined thresholds, respectively. The maximum of EE with a fractional objective function is transformed into problem $\mathcal{P}2$ in (17) with a subtractive objective function [39], [40]. We notice that optimal EE λ^* can be obtained iteratively until convergence. However, it still leads to non-linearity and

$$\delta_{1\to2,m} = \left|\frac{\sin\left[\frac{\pi}{Q}f' - \Big((k \bmod F_2)\,Q - \phi_m F_1 - 1\Big)\right]}{\sin\left[\frac{\pi}{F_1}f' - \Big((k \bmod F_2)\,Q - 2\phi_m F_1 - 1\Big)\right]}\right|^2, \tag{8}$$

$$\delta^{(1)}_{2\to1,m} = \left|\frac{\sin\left[\frac{\pi}{Q}\Big(1+(1-Q)\,\gamma\Big)\Big(f'Q - (k \bmod F_1) - \phi_m F_1 - 1\Big)\right]}{\sin\left[\frac{\pi}{F_1}\Big(f'Q - (k \bmod F_1) - 1\Big)\right]}\right|^2, \tag{9}$$

$$\delta^{(2)}_{2\to1,m} = \left|\frac{\sin\left[\frac{\pi}{Q}\,(1+\gamma)\,\Big(f'Q - (k \bmod F_1) - \phi_m F_1 - 1\Big)\right]}{\sin\left[\frac{\pi}{F_1}\Big(f'Q - (k \bmod F_1) - 1\Big)\right]}\right|^2. \tag{10}$$

$$\begin{aligned}(\mathcal{P}1):\ &\max_{\boldsymbol{P},\boldsymbol{\rho},\boldsymbol{\alpha}}\ \Lambda(\boldsymbol{P},\boldsymbol{\rho},\boldsymbol{\alpha}) && (15a)\\ &\text{s.t.}\quad R^n(\boldsymbol{P},\boldsymbol{\rho},\boldsymbol{\alpha}) \geq R^e_{\min},\quad \forall n\in\mathcal{N}_e, && (15b)\\ &\quad R^n(\boldsymbol{P},\boldsymbol{\rho},\boldsymbol{\alpha}) \geq R^u_{\min},\quad \forall n\in\mathcal{N}_u, && (15c)\\ &\quad \Theta(l,i,k)\rho^{n,l}_{i,k} \leq \tau_e,\quad \forall n\in\mathcal{N}_e,\quad l\in\mathcal{L},\quad i\in\mathcal{I},\quad k\in\mathcal{K}, && (15d)\\ &\quad \Theta(l,i,k)\rho^{n,l}_{i,k} \leq \tau_u,\quad \forall n\in\mathcal{N}_u,\quad l\in\mathcal{L},\quad i\in\mathcal{I},\quad k\in\mathcal{K}, && (15e)\\ &\quad 0 \leq P^{n,l}_{i,k} \leq P_{\max},\quad \forall n\in\mathcal{N},\quad l\in\mathcal{L},\quad i\in\mathcal{I},\quad k\in\mathcal{K}, && (15f)\\ &\quad 0 \leq \sum_{n\in\mathcal{N}}\sum_{l\in\mathcal{L}}\sum_{i\in\mathcal{I}}\sum_{k\in\mathcal{K}} P^{n,l}_{i,k} \leq P^{\text{tot}}_{\max}, && (15g)\\ &\quad \rho^{n,l}_{i,k} \in \{0,1\},\quad \forall n\in\mathcal{N},\quad l\in\mathcal{L},\quad i\in\mathcal{I},\quad k\in\mathcal{K}, && (15h)\\ &\quad \alpha_{l,m} \in \{0,1\},\quad \forall l\in\mathcal{L},\quad m\in\mathcal{M}, && (15i)\\ &\quad \sum_{m\in\mathcal{M}} \alpha_{l,m} = 1,\quad \forall l\in\mathcal{L}, && (15j)\\ &\quad \sum_{n\in\mathcal{N}} \rho^{n,l}_{i,k} = \sum_{m\in\mathcal{M}} \alpha_{l,m}\omega^m_{i,k} \in \{0,1\},\quad \forall l\in\mathcal{L},\quad i\in\mathcal{I},\quad k\in\mathcal{K}. && (15k)\end{aligned}$$

non-convexity in the first term of throughput function which is addressed as belows.

2) Auxiliary of Coupled Variables: We can observe from SINR in (11) that the coupled term regarding all policies take place as $P_{i,k}^{n,l}\rho_{i,k}^{n,l}\sum_{m\in\mathcal{M}}\alpha_{l,m}\omega_{i,k}^{m}$ containing both continuous and discrete variables. To deal with this, we define an auxiliary parameter denoted by $\widehat{P}_{i,k}^{n,l}$ as

$$\widehat{P}_{i,k}^{n,l} = \begin{cases} 0, & \text{if } \rho_{i,k}^{n,l}\sum_{m\in\mathcal{M}}\alpha_{l,m}\omega_{i,k}^{m}=0, \\ P_{i,k}^{n,l}\rho_{i,k}^{n,l}\sum_{m\in\mathcal{M}}\alpha_{l,m}\omega_{i,k}^{m}, & \text{otherwise.} \end{cases} \tag{19}$$

Note that (19) implies that we transmit data with power $P_{i,k}^{n,l}$ once the specific RB and NBR is selected. To ensure the relationship stated above, a new constraint related to power constraint (15f) should be equivalently introduced as

$$0 \le \widehat{P}_{i,k}^{n,l} \overset{(a)}{\le} \left(\rho_{i,k}^{n,l}\sum_{m\in\mathcal{M}}\alpha_{l,m}\omega_{i,k}^{m}\right)P_{\max} \overset{(b)}{\le} P_{\max}, \tag{20}$$

where (a) holds according to (19) and (b) follows the fact that $\left(\rho_{i,k}^{n,l}\sum_{m\in\mathcal{M}}\alpha_{l,m}\omega_{i,k}^{m}\right)\le 1$. Note that we neglect the similar procedure for total power constraint in (15g). Therefore, we can deduce the following lemma regarding the upper bound of INI.

Lemma 1: According to the defined auxiliary parameter of power $\widehat{P}_{i,k}^{n,l}$, the MN-based INI function in (6) *and* (7) *can be derived to be upper bounded by*

$$\widehat{INI}_{1\to 2,k}^{l} = \sum_{n=1}^{N}\sum_{f'=1}^{F_1}\frac{\widehat{P}_{1,f'}^{n,l}}{F_1F_2}\left[\sum_{m\in\mathcal{M}}\left(\delta_{1\to 2,m}\right)^{\sigma}\right]^{\frac{1}{\sigma}}, \tag{21}$$

and

$$\begin{aligned}\widehat{INI}_{2\to 1,k}^{l} &= \sum_{n=1}^{N}\sum_{f'=1}^{F_2}\frac{\widehat{P}_{2,f'}^{n,l}}{F_1F_2}\left[\sum_{m\in\mathcal{M}}\left(\delta_{2\to 1,m}^{(1)}\right)^{\sigma}\right]^{\frac{1}{\sigma}} \\ &\quad + \sum_{n=1}^{N}\sum_{f'=1}^{F_2}\sum_{q=1}^{Q-1}\frac{\widehat{P}_{2,F_2q+f'}^{n,l}}{F_1F_2}\left[\sum_{m\in\mathcal{M}}\left(\delta_{2\to 1,m}^{(2)}\right)^{\sigma}\right]^{\frac{1}{\sigma}},\end{aligned} \tag{22}$$

where σ is a positive constant indicating the tightness compared to the original INI functions. The parameters of $\delta_{1\to 2,m}$, $\delta_{2\to 1,m}^{(1)}$ and $\delta_{2\to 1,m}^{(2)}$ are defined in (8)–(10)*, respectively.*

Proof: Let us first consider the INI function of $INI_{1\to 2,k}^{l}$. Based on the Holder inequality, we can derive the upper bound of the third summation in $INI_{1\to 2,k}^{l}$ as

$$\begin{aligned}&\sum_{m\in\mathcal{M}}\alpha_{l,m}\omega_{1,f'}^{m}\delta_{1\to 2,m} \\ &\le \left[\sum_{m\in\mathcal{M}}\left(\alpha_{l,m}\omega_{1,f'}^{m}\right)^{\sigma'}\right]^{\frac{1}{\sigma'}}\left[\sum_{m\in\mathcal{M}}\left(\delta_{1\to 2,m}\right)^{\sigma}\right]^{\frac{1}{\sigma}} \\ &\overset{(a)}{=} \sum_{m\in\mathcal{M}}\alpha_{l,m}\omega_{1,f'}^{m}\left[\sum_{m\in\mathcal{M}}\left(\delta_{1\to 2,m}\right)^{\sigma}\right]^{\frac{1}{\sigma}},\end{aligned} \tag{23}$$

where $\sigma' > 1$ satisfying $\frac{1}{\sigma}+\frac{1}{\sigma'}=1$. The equality (a) follows the fact that $\left[\sum_{m\in\mathcal{M}}\left(\alpha_{l,m}\omega_{1,f'}^{m}\right)^{\sigma'}\right]^{\frac{1}{\sigma'}} = \left(\sum_{m\in\mathcal{M}}\alpha_{l,m}\omega_{1,f'}^{m}\right)^{\frac{1}{\sigma'}} = \sum_{m\in\mathcal{M}}\alpha_{l,m}\omega_{1,f'}^{m}$ since $\alpha_{l,m}\omega_{1,f'}^{m}$ is the multiplication of two binary decisions. Substituting the term $P_{1,f'}^{n,l}\rho_{i,k}^{n,l}\sum_{m\in\mathcal{M}}\alpha_{l,m}\omega_{1,f'}^{m}\delta_{1\to 2,m}$ in (6) by (23) yields the upper bound of $INI_{1\to 2,k}^{l}$ as $\widehat{INI}_{1\to 2,k}^{l}$ in (21). Additionally, we can prove the upper bound of $INI_{2\to 1,k}^{l}$ as $\widehat{INI}_{2\to 1,k}^{l}$ in (22) according to (23), which is omitted here due to similar derivations. This completes the proof. □

Remark 1: The functions of ICI in (4) *and ISI in* (5) *are respectively substituted by $\widehat{ICI}_{i,k}^{l}$ and $\widehat{ISI}_{i,k}^{n,l}$ having equivalent values to the original functions.*

Based on (19), Lemma 1 and Remark 1, we can attain the lower bound of SINR in (11) as

$$\widehat{\Gamma}_{i,k}^{n,l} = \frac{\widehat{P}_{i,k}^{n,l}\left|h_{i,k}^{n,l}\right|^2}{\widehat{ICI}_{i,k}^{l}+\widehat{ISI}_{i,k}^{n,l}+\widehat{INI}_{i'\to i,k}^{l}+N_0\cdot\Delta f_i}. \tag{24}$$

The corresponding throughput function $R^n(\widehat{\boldsymbol{P}})$ and power consumption $P^{n,l}(\widehat{\boldsymbol{P}})$ can also be acquired in a similar manner by replacing auxiliary parameters in (19) which are given by

$$R^n(\widehat{\boldsymbol{P}}) = \sum_{l\in\mathcal{L}}\sum_{i\in\mathcal{I}}\sum_{k\in\mathcal{K}}T_i\cdot\Delta f_i\cdot\log_2\left(1+\widehat{\Gamma}_{i,k}^{n,l}\right), \tag{25}$$

$$P^{n,l}(\widehat{\boldsymbol{P}}) = \sum_{i\in\mathcal{I}}\sum_{k\in\mathcal{K}}\frac{T_i}{T_1}\cdot\eta_{\text{PA}}\widehat{P}_{i,k}^{n,l}+P_{\text{circuit}}. \tag{26}$$

Subsequently, the problem $\mathcal{P}2$ in (17) is transformed into the optimization problem formulated as

$$\begin{aligned}(\mathcal{P}3): \max_{\widehat{\boldsymbol{P}},\boldsymbol{\rho},\boldsymbol{\alpha}} \ & \sum_{n\in\mathcal{N}}R^n(\widehat{\boldsymbol{P}})-\lambda\left(\sum_{n\in\mathcal{N}}\sum_{l\in\mathcal{L}}P^{n,l}(\widehat{\boldsymbol{P}})\right) && \text{(27a)} \\ \text{s.t.} \ & \text{(15d), (15e), (15h)–(15k),} && \text{(27b)} \\ & R^n(\widehat{\boldsymbol{P}})\ge R_{\min}^{e}, \quad \forall n\in\mathcal{N}_e, && \text{(27c)} \\ & R^n(\widehat{\boldsymbol{P}})\ge R_{\min}^{u}, \quad \forall n\in\mathcal{N}_u, && \text{(27d)} \\ & 0\le\widehat{P}_{i,k}^{n,l}\le P_{\max}, \\ & \forall n\in\mathcal{N}, \quad l\in\mathcal{L}, \quad i\in\mathcal{I}, \quad k\in\mathcal{K}, && \text{(27e)} \\ & 0\le\sum_{n\in\mathcal{N}}\sum_{l\in\mathcal{L}}\sum_{i\in\mathcal{I}}\sum_{k\in\mathcal{K}}\widehat{P}_{i,k}^{n,l}\le P_{\max}^{\text{tot}}. && \text{(27f)}\end{aligned}$$

Note that λ is a predefined penalty parameter derived from $\mathcal{P}2$. We can have the following proposition regarding the problem in (27).

Theorem 1: The maximization of problem $\mathcal{P}2$ in (17) *is equivalent to optimizing its lower bound in problem $\mathcal{P}3$ in* (27)*.*

Proof: According to Lemma 1 and Remark 1, it can be inferred that $\widehat{\Gamma}_{i,k}^{n,l}\le\Gamma_{i,k}^{n,l}$ due to the fact that $\widehat{INI}_{i'\to i,k}^{l}\ge INI_{i'\to i,k}^{l}$, $\widehat{ICI}_{i,k}^{l}=ICI_{i,k}^{l}$ and $\widehat{ISI}_{i,k}^{l}=ISI_{i,k}^{l}$. The logarithmic function of throughput is monotonically increasing with the variable of SINR $\widehat{\Gamma}_{i,k}^{n,l}$, and therefore we have $R^n(\boldsymbol{P},\boldsymbol{\rho},\boldsymbol{\alpha})\ge R^n(\widehat{\boldsymbol{P}})$. Furthermore, $P^{n,l}(\widehat{\boldsymbol{P}})$ is equivalent to the original power consumption of $P^{n,l}(\boldsymbol{P},\boldsymbol{\rho},\boldsymbol{\alpha})$. As a

result, the objective function (27a) is the lower bound of that in (17). Based on a similar derivation, we can prove that QoS constraints (27c) and (27d) are also the corresponding subsets of original ones in (15b) and (15c), respectively. While, the power constraints (27e) and (27f) possess the same feasible region as (15f) and (15g), respectively. We can thus prove that the maximization of problem $\mathcal{P}2$ in (17) is equivalent to optimizing its lower bound in problem $\mathcal{P}3$ in (27), which completes the proof. □

3) Integer Relaxation of Binary Variables: Motivated by [41], [42], to deal with the binary variables problem, we relax the RB and NBR assignments within the region between 0 and 1, i.e., the policies of variable constraints in (15h) and (15i) are alternatively expressed as

$$\widehat{\boldsymbol{\rho}} = \left\{0 \leq \widehat{\rho}_{i,k}^{n,l} \leq 1 |\ \forall n \in \mathcal{N}, l \in \mathcal{L}, i \in \mathcal{I}, k \in \mathcal{K}\right\}, \quad (28)$$

$$\widehat{\boldsymbol{\alpha}} = \left\{0 \leq \widehat{\alpha}_{l,m} \leq 1 |\ \forall l \in \mathcal{L}, m \in \mathcal{M}\right\}, \quad (29)$$

respectively. Inspired by [43], in order to approximate the continuous relaxed variables to zero and one, we design two penalty functions as auxiliary constraints which are given by

$$G_1(\widehat{\boldsymbol{\rho}}) = \sum_{n\in\mathcal{N}}\sum_{l\in\mathcal{L}}\sum_{i\in\mathcal{I}}\sum_{k\in\mathcal{K}} \widehat{\rho}_{i,k}^{n,l}\left(1-\widehat{\rho}_{i,k}^{n,l}\right) \leq 0, \quad (30)$$

$$G_2(\widehat{\boldsymbol{\alpha}}) = \sum_{l\in\mathcal{L}}\sum_{m\in\mathcal{M}} \widehat{\alpha}_{l,m}\left(1-\widehat{\alpha}_{l,m}\right) \leq 0, \quad (31)$$

where problem $\mathcal{P}3$ in (27) will stay unchanged as proven in the following proposition.

Proposition 1: The problem $\mathcal{P}3$ stays unchanged with the employment of integer relaxation, i.e., substitute discrete decisions of $\{\boldsymbol{\rho}, \boldsymbol{\alpha}\}$ by $\{\widehat{\boldsymbol{\rho}}, \widehat{\boldsymbol{\alpha}}\}$ under constraints (30) *and* (31)*.*

Proof: We can infer from (30) that $\widehat{\rho}_{i,k}^{n,l}\left(1-\widehat{\rho}_{i,k}^{n,l}\right)$ is a concave function which possesses two roots as $\widehat{\rho}_{i,k}^{n,l} \in \{0,1\}$. Accordingly, inequality (30) ensures the regions of $\widehat{\rho}_{i,k}^{n,l} \leq 0$ and $\widehat{\rho}_{i,k}^{n,l} \geq 1$. Leveraging the solution of (30) and $0 \leq \widehat{\rho}_{i,k}^{n,l} \leq 1$ in (28) yields $\widehat{\rho}_{i,k}^{n,l} \in \{0,1\}$, which sustains the property of the original discrete variable $\rho_{i,k}^{n,l}$. By employing the same derivation stated above, we can deduce that $\widehat{\alpha}_{i,k}^{n,l} \in \{0,1\}$ considering (29) and (31). As a result, we can conclude that problem $\mathcal{P}3$ is unchanged by using integer relaxation of (28) and (29) with additional auxiliary constraints (30) and (31), respectively. This completes the proof. □

We define that $\mathcal{D}'$ denotes a set consisting of all constraints (27b)–(27f), and integer relaxation in (28) and (29). Benefited by relaxing discrete variables, the optimization problem in (27) is equivalent to the following one

$$\max_{\{\widehat{\boldsymbol{P}},\widehat{\boldsymbol{\rho}},\widehat{\boldsymbol{\alpha}}\}\in\mathcal{D}'} \quad \sum_{n\in\mathcal{N}} R^n(\widehat{\boldsymbol{P}}) - \lambda\left(\sum_{n\in\mathcal{N}}\sum_{l\in\mathcal{L}} P^{n,l}(\widehat{\boldsymbol{P}})\right) \quad (32a)$$

$$\text{s.t.} \quad G_1(\widehat{\boldsymbol{\rho}}) \leq 0, \quad (32b)$$

$$G_2(\widehat{\boldsymbol{\alpha}}) \leq 0. \quad (32c)$$

Note that the constraints (32b) and (32c) are non-convex, which can be resolved with the employment of abstract Lagrangian duality [44]. We transform both constraints into the respective penalty terms, and the abstract Lagrangian objective is given by

$$\begin{aligned}&\Upsilon(\widehat{\boldsymbol{P}}, \widehat{\boldsymbol{\rho}}, \widehat{\boldsymbol{\alpha}}, \beta_\rho, \beta_\alpha)\\ &= \sum_{n\in\mathcal{N}} R^n(\widehat{\boldsymbol{P}}) - \lambda\left(\sum_{n\in\mathcal{N}}\sum_{l\in\mathcal{L}} P^{n,l}(\widehat{\boldsymbol{P}})\right)\\ &\quad - \beta_\rho G_1(\widehat{\boldsymbol{\rho}}) - \beta_\alpha G_2(\widehat{\boldsymbol{\alpha}}),\end{aligned} \quad (33)$$

where $\beta_\rho \geq 0$ and $\beta_\alpha \geq 0$ are denoted as penalty constants. The transformed problem can be formulated as a primal problem as

$$(\mathcal{P}4): \max_{\{\widehat{\boldsymbol{P}},\widehat{\boldsymbol{\rho}},\widehat{\boldsymbol{\alpha}}\}\in\mathcal{D}'} \min_{\beta_\rho,\beta_\alpha} \Upsilon(\widehat{\boldsymbol{P}}, \widehat{\boldsymbol{\rho}}, \widehat{\boldsymbol{\alpha}}, \beta_\rho, \beta_\alpha). \quad (34)$$

Note that the primal problem $\mathcal{P}4$ is in a form of max-min with β_ρ and β_α existing in the minimization operator. This is because minimization of the negative part of the induced penalties in Lagrangian objective in (33) aims for sustaining the constraints in (28)–(31) and satisfying the non-penalized problem in (32).

Theorem 2: The transformed problem $\mathcal{P}4$ in (34) *is equivalent to the unrelaxed problem $\mathcal{P}3$ of* (27) *with the attained sufficiently large values of β_ρ and β_α.*

Proof: We can learn from Proposition 1 that the problem in (32) is unchanged by introducing integer relaxation with its primal problem of $\mathcal{P}4$ in (34). While, the corresponding dual problem is a min-max optimization as

$$\min_{\beta_\rho,\beta_\alpha} \max_{\{\widehat{\boldsymbol{P}},\widehat{\boldsymbol{\rho}},\widehat{\boldsymbol{\alpha}}\}\in\mathcal{D}'} \Upsilon(\widehat{\boldsymbol{P}}, \widehat{\boldsymbol{\rho}}, \widehat{\boldsymbol{\alpha}}, \beta_\rho, \beta_\alpha). \quad (35)$$

We define the optimum of primal problem in (34) as p^*, whereas the optimum for its dual one (35) is denoted as d^*. According to the weak duality theorem, we can obtain the following relationship as

$$\begin{aligned}p^* &= \max_{\{\widehat{\boldsymbol{P}},\widehat{\boldsymbol{\rho}},\widehat{\boldsymbol{\alpha}}\}\in\mathcal{D}'} \min_{\beta_\rho,\beta_\alpha} \Upsilon(\widehat{\boldsymbol{P}}, \widehat{\boldsymbol{\rho}}, \widehat{\boldsymbol{\alpha}}, \beta_\rho, \beta_\alpha)\\ &\leq \min_{\beta_\rho,\beta_\alpha} \nu(\beta_\rho, \beta_\alpha) = d^*,\end{aligned} \quad (36)$$

where the inner maximization problem in the dual problem of (35) is defined as $\nu(\beta_\rho, \beta_\alpha) \triangleq \max_{\{\widehat{\boldsymbol{P}},\widehat{\boldsymbol{\rho}},\widehat{\boldsymbol{\alpha}}\}\in\mathcal{D}'} \Upsilon(\widehat{\boldsymbol{P}}, \widehat{\boldsymbol{\rho}}, \widehat{\boldsymbol{\alpha}}, \beta_\rho, \beta_\alpha)$. Therefore, we have four possible cases to be discussed in the followings.

- **Case 1**: Suppose that we have $G_1(\widehat{\boldsymbol{\rho}}) = G_2(\widehat{\boldsymbol{\alpha}}) = 0$. Substituting β_ρ^* and β_α^* as feasible solutions of the dual problem yields

$$\begin{aligned}d^* &= \nu(\beta_\rho^*, \beta_\alpha^*)\\ &= \max_{\{\widehat{\boldsymbol{P}},\widehat{\boldsymbol{\rho}},\widehat{\boldsymbol{\alpha}}\}\in\mathcal{D}'} \min_{\beta_\rho,\beta_\alpha} \Upsilon(\widehat{\boldsymbol{P}}, \widehat{\boldsymbol{\rho}}, \widehat{\boldsymbol{\alpha}}, \beta_\rho, \beta_\alpha)\\ &= p^*.\end{aligned} \quad (37)$$

  We can observe from (33) that $\nu(\beta_\rho, \beta_\alpha)$ is a monotonically-decreasing function with respect to both β_ρ and β_α. Because $d^* = \min_{\beta_\rho,\beta_\alpha} \nu(\beta_\rho, \beta_\alpha)$ based on (36), we can derive $d^* = \nu(\beta_\rho, \beta_\alpha),\ \forall \beta_\rho \geq \beta_\rho^*, \beta_\alpha \geq \beta_\alpha^*$, which implies that the solution of $\mathcal{P}4$ provides the optimal one of unrelaxed problem $\mathcal{P}3$ for sufficiently large values of β_ρ and β_α for $\beta_\rho \geq \beta_\rho^*$ and $\beta_\alpha \geq \beta_\alpha^*$, respectively.

- **Case 2**: Let $G_2(\widehat{\boldsymbol{\alpha}}) = 0$ and consider the case of $0 \leq \widehat{\rho}_{i,k}^{n,l} \leq 1$, it reveals that $G_1(\widehat{\boldsymbol{\rho}}) \geq 0$ holds accordingly. Based on Case 1, we can have a deduction that the converted problem is unchanged via sufficiently large β_α with fixed β_ρ. Therefore, we only need to take β_ρ into account. Since $\nu(\beta_\rho, \beta_\alpha)$ is monotonically decreasing, the optimum $\nu(\beta_\rho^*, \beta_\alpha)$ will tend to approach $-\infty$, which contradicts the derivation of weak duality in (36), i.e., it should be $G_1(\widehat{\boldsymbol{\rho}}) = 0$.
- **Case 3**: Employing the similar proof in Case 2 by setting $G_1(\widehat{\boldsymbol{\rho}}) = 0$ with $0 \leq \widehat{\alpha}_{i,k}^{n,l} \leq 1$ will result in $\nu(\beta_\rho, \beta_\alpha^*) \to -\infty$. That is, we can conclude $G_2(\widehat{\boldsymbol{\alpha}}) = 0$ under the inconsistent assumption same as that in Case 2.
- **Case 4**: By leveraging results of Cases 2 and 3, we consider the situation of $0 \leq \widehat{\rho}_{i,k}^{n,l} \leq 1$ and $0 \leq \widehat{\alpha}_{i,k}^{n,l} \leq 1$ which provides $G_1(\widehat{\boldsymbol{\rho}}) \geq 0$ and $G_2(\widehat{\boldsymbol{\alpha}}) \geq 0$, respectively. Accordingly, $\nu(\beta_\rho^*, \beta_\alpha^*)$ will have a tendency of approaching $-\infty$, which also conflicts duality in (36).

Based on Cases 1 to 4, we can conclude that the transformed problem $\mathcal{P}4$ in (34) is equivalent to the unrelaxing problem $\mathcal{P}3$ of (27) with sufficiently large values of β_ρ and β_α. This completes the proof. □

4) Approximation of Non-Concavity: However, we can know from problem $\mathcal{P}4$ in (34) that the objective function $\Upsilon(\widehat{\boldsymbol{P}}, \widehat{\boldsymbol{\rho}}, \widehat{\boldsymbol{\alpha}}, \beta_\rho, \beta_\alpha)$ performs a non-concave form. Hence, we employ D.C. approximation [45] to convert non-convex problem into a solvable convex one. First of all, we rewrite the throughput function into a subtractive form as $R^n(\widehat{\boldsymbol{P}}) = R_1^n(\widehat{\boldsymbol{P}}) - R_2^n(\widehat{\boldsymbol{P}})$, where

$$R_1^n(\widehat{\boldsymbol{P}}) = \sum_{l\in\mathcal{L}}\sum_{i\in\mathcal{I}}\sum_{k\in\mathcal{K}} T_i \Delta f_i \log_2\left(\widehat{P}_{i,k}^{n,l}\left|h_{i,k}^{n,l}\right|^2 + \widehat{ICI}_{i,k}^{l} + \widehat{ISI}_{i,k}^{n,l} + \widehat{INI}_{i'\to i,k}^{l} + N_0\Delta f_i\right), \tag{38}$$

$$R_2^n(\widehat{\boldsymbol{P}}) = \sum_{l\in\mathcal{L}}\sum_{i\in\mathcal{I}}\sum_{k\in\mathcal{K}} T_i \Delta f_i \log_2\left(\widehat{ICI}_{i,k}^{l} + \widehat{ISI}_{i,k}^{n,l} + \widehat{INI}_{i'\to i,k}^{l} + N_0\Delta f_i\right). \tag{39}$$

Therefore, according to (38) and (39), we partition terms in (33) by defining an alternative D.C. objective function as $F(\widehat{\boldsymbol{P}}, \widehat{\boldsymbol{\rho}}, \widehat{\boldsymbol{\alpha}}) = F_1(\widehat{\boldsymbol{P}}, \widehat{\boldsymbol{\rho}}, \widehat{\boldsymbol{\alpha}}) - F_2(\widehat{\boldsymbol{P}}, \widehat{\boldsymbol{\rho}}, \widehat{\boldsymbol{\alpha}})$, where

$$F_1(\widehat{\boldsymbol{P}}, \widehat{\boldsymbol{\rho}}, \widehat{\boldsymbol{\alpha}}) = \sum_{n\in\mathcal{N}} R_1^n(\widehat{\boldsymbol{P}}) - \lambda\left(\sum_{n\in\mathcal{N}}\sum_{l\in\mathcal{L}} P^{n,l}(\widehat{\boldsymbol{P}})\right), \tag{40}$$

$$F_2(\widehat{\boldsymbol{P}}, \widehat{\boldsymbol{\rho}}, \widehat{\boldsymbol{\alpha}}) = \sum_{n\in\mathcal{N}} R_2^n(\widehat{\boldsymbol{P}}) + \beta_\rho G_1(\widehat{\boldsymbol{\rho}}) + \beta_\alpha G_2(\widehat{\boldsymbol{\alpha}}). \tag{41}$$

We can infer that concavity property does not exactly hold in $F(\widehat{\boldsymbol{P}}, \widehat{\boldsymbol{\rho}}, \widehat{\boldsymbol{\alpha}})$ due to two subtractive concave functions. Therefore, we employ first-order Taylor approximation [46] on $F_2(\widehat{\boldsymbol{P}}, \widehat{\boldsymbol{\rho}}, \widehat{\boldsymbol{\alpha}})$ to transform concave functions into affine ones. We first approximate the term $R_2^n(\widehat{\boldsymbol{P}})$ which can be derived by

$$\widetilde{R}_2^n(\widehat{\boldsymbol{P}}[j]) = R_2^n(\widehat{\boldsymbol{P}}[j-1]) + \nabla_{\widehat{\boldsymbol{P}}}^T R_2^n(\widehat{\boldsymbol{P}}[j-1]) \cdot \Big(\widehat{\boldsymbol{P}}[j] - \widehat{\boldsymbol{P}}[j-1]\Big), \tag{42}$$

where $\nabla_{\widehat{\boldsymbol{P}}}^T R_2^n(\widehat{\boldsymbol{P}})$ indicates the first-order partial derivative of $R_2^n(\widehat{\boldsymbol{P}})$ with respect to $\widehat{\boldsymbol{P}}$. Note that T is transpose operation, whilst index j means the iteration count. The element of partial derivative of $\nabla_{\widehat{\boldsymbol{P}}}^T R_2^n(\widehat{\boldsymbol{P}})$ is further expressed by (43), shown at the bottom of the next page, where the related parameters are given by the equation can be derived, shown at the bottom of next page. Similarly, we can derive the remaining terms as

$$\widetilde{G}_1(\widehat{\boldsymbol{\rho}}[j]) = G_1(\widehat{\boldsymbol{\rho}}[j-1]) + \nabla_{\widehat{\boldsymbol{\rho}}}^T G_1(\widehat{\boldsymbol{\rho}}[j-1]) \cdot \Big(\widehat{\boldsymbol{\rho}}[j] - \widehat{\boldsymbol{\rho}}[j-1]\Big), \tag{44}$$

$$\widetilde{G}_2(\widehat{\boldsymbol{\alpha}}[j]) = G_2(\widehat{\boldsymbol{\alpha}}[j-1]) + \nabla_{\widehat{\boldsymbol{\alpha}}}^T G_2(\widehat{\boldsymbol{\alpha}}[j-1]) \cdot \Big(\widehat{\boldsymbol{\alpha}}[j] - \widehat{\boldsymbol{\alpha}}[j-1]\Big), \tag{45}$$

where the elements of partial derivatives in (44) and (45) are derived as $\frac{\partial G_1(\widehat{\boldsymbol{\rho}})}{\partial \widehat{\rho}_{i,k}^{n,l}} = 1 - 2\widehat{\rho}_{i,k}^{n,l}$ and $\frac{\partial G_2(\widehat{\boldsymbol{\alpha}})}{\partial \widehat{\alpha}_{l,m}} = 1 - 2\widehat{\alpha}_{l,m}$, respectively. Based on (42), (44) and (45), we can approximate $F_2(\widehat{\boldsymbol{P}}, \widehat{\boldsymbol{\rho}}, \widehat{\boldsymbol{\alpha}})$ as

$$\widetilde{F}_2(\widehat{\boldsymbol{P}}, \widehat{\boldsymbol{\rho}}, \widehat{\boldsymbol{\alpha}}) = \widetilde{R}_2^n(\widehat{\boldsymbol{P}}) + \beta_\rho \widetilde{G}_1(\widehat{\boldsymbol{\rho}}) + \beta_\alpha \widetilde{G}_2(\widehat{\boldsymbol{\alpha}}). \tag{46}$$

We can then define the new objective as $\widetilde{F}(\widehat{\boldsymbol{P}}, \widehat{\boldsymbol{\rho}}, \widehat{\boldsymbol{\alpha}}) = F_1(\widehat{\boldsymbol{P}}, \widehat{\boldsymbol{\rho}}, \widehat{\boldsymbol{\alpha}}) - \widetilde{F}_2(\widehat{\boldsymbol{P}}, \widehat{\boldsymbol{\rho}}, \widehat{\boldsymbol{\alpha}})$. Accordingly, we can transform $\mathcal{P}4$ into the following problem formulated as

$$(\mathcal{P}5): \max_{\widehat{\boldsymbol{P}}, \widehat{\boldsymbol{\rho}}, \widehat{\boldsymbol{\alpha}}} \quad \widetilde{F}(\widehat{\boldsymbol{P}}, \widehat{\boldsymbol{\rho}}, \widehat{\boldsymbol{\alpha}}) \tag{47a}$$

$$\text{s.t.} \quad (15\text{d}), (15\text{e}), (15\text{j}), (15\text{k}), (27\text{e}), (27\text{f}), (28), (29), \tag{47b}$$

$$\widetilde{R}^n(\widehat{\boldsymbol{P}}) \geq R_{\min}^e, \quad \forall n \in \mathcal{N}_e, \tag{47c}$$

$$\widetilde{R}^n(\widehat{\boldsymbol{P}}) \geq R_{\min}^u, \quad \forall n \in \mathcal{N}_u, \tag{47d}$$

where $\widetilde{R}^n(\widehat{\boldsymbol{P}}) = R_1^n(\widehat{\boldsymbol{P}}) - \widetilde{R}_2^n(\widehat{\boldsymbol{P}})$. The following theorem demonstrates that $\mathcal{P}5$ preserves concavity property.

Theorem 3: With the aid of D.C. and Taylor's first-order approximation, the transformed problem $\mathcal{P}5$ is convex with a concave objective and convex constraints. Moreover, converted QoS constraints preserve the original throughput satisfaction.

Proof: Based on D.C. and Taylor's first-order approximation, we can infer from (42), (44) and (45) that the respective solutions of $\widetilde{R}_2^n(\widehat{\boldsymbol{P}})$, $\widetilde{G}_1(\widehat{\boldsymbol{\rho}})$ and $\widetilde{G}_2(\widehat{\boldsymbol{\alpha}})$ are given at previous iteration $j-1$, whereas the only variables are those to be determined at j-th iteration, which results in affine functions. Therefore, $F(\widehat{\boldsymbol{P}}, \widehat{\boldsymbol{\rho}}, \widehat{\boldsymbol{\alpha}})$ is concave owing to the summation of concave function $\widetilde{F}_1(\widehat{\boldsymbol{P}})$ and affine one $\widetilde{F}_2(\widehat{\boldsymbol{P}})$. Moreover, concave function of $R^n(\widehat{\boldsymbol{P}})$ provokes convex constraints of (47c) and (47d). Therefore, with the aid of D.C. and Taylor's first-order approximation, the transformed problem $\mathcal{P}5$ is convex with a concave objective and convex constraints. Due to the concave property of $R_2^n(\widehat{\boldsymbol{P}})$ function in (39), we can know that the inequality $R_2^n(\widehat{\boldsymbol{P}}) \leq \widetilde{R}_2^n(\widehat{\boldsymbol{P}})$ holds. Accordingly, it can be deduced that

$$R^n(\widehat{\boldsymbol{P}}) \geq \widetilde{R}^n(\widehat{\boldsymbol{P}}) \tag{48}$$

By comparing (27c), (27d), (47c), (47d) and (48), we can derive $R^n(\widehat{\boldsymbol{P}}) \geq \widetilde{R}^n(\widehat{\boldsymbol{P}}) \geq R_{\min}^x$, $\forall n \in \mathcal{N}_x$, where

$x \in \{e, u\}$ indicates either eMBB or URLLC services. As a result, the new QoS constraints provide a smaller feasible solution set of the transformed problem $\mathcal{P}5$, which preserves the original throughput satisfaction. This completes the proof. □

B. Proposed MNPRA Algorithm

We can observe from Theorem 3 that problem $\mathcal{P}5$ is a convex problem, which can be resolved through arbitrary convex optimization tools. Owing to the transformations stated above, we have to iteratively acquire the candidate solution of the power $\widehat{\boldsymbol{P}}$, RB indicator $\widehat{\boldsymbol{\rho}}$ and NBR assignment $\widehat{\boldsymbol{\alpha}}$ in $\mathcal{P}5$ until convergence. We notice that the solution of $\mathcal{P}5$ is equivalently applied in the original problem $\mathcal{P}1$ owing to introduced auxiliary constraints. The overall MNPRA algorithm is demonstrated in Algorithm 1. First, we initialize the required inputs including channel gain $h_{i,k}^{n,l}, \forall n \in \mathcal{N}, l \in \mathcal{L}, i \in \mathcal{I}, k \in \mathcal{K}$, iteration index $j = 1$, temporary EE parameter $\lambda[j]$ and initial policy set $\{\boldsymbol{P}[j], \boldsymbol{\rho}[j], \boldsymbol{\alpha}[j]\}$. The EE approximation is performed at outer loop by calculating $\lambda[j]$ in (18). On the other hand, the inner loop conducts convex problem resolution to derive the optimal solution from the convex problem $\mathcal{P}5$ in (47). Note that both iterations converge when the difference of the objective between two successive iterations is smaller than a given threshold. That is,

$$\lambda[j] - \lambda[j-1] \leq \kappa_{out} \tag{49}$$

is for EE approximation at outer loop, whereas

$$\widetilde{F}(\widehat{\boldsymbol{P}}[j'], \widehat{\boldsymbol{\rho}}[j'], \widehat{\boldsymbol{\alpha}}[j']) - \widetilde{F}(\widehat{\boldsymbol{P}}[j'-1], \widehat{\boldsymbol{\rho}}[j'-1], \widehat{\boldsymbol{\alpha}}[j'-1]) \leq \kappa_{in} \tag{50}$$

holds for convergence of the inner loop of Algorithm 1. We also note that the maximum allowable iterations are upper bounded by T_{in} and T_{out} for inner/outer loops, respectively. Note that as our initial feasible policy of Algorithm 1, we follow the random assignment satisfying the conditions when $\min\ R^n(P_{\max}, \boldsymbol{\rho}, \boldsymbol{\alpha}) \geq R_{\min}^x$, $\max\ \Theta(l,i,k)\rho_{i,k}^{n,l} \leq \tau_x$, and $\sum_{l\in\mathcal{L}}\sum_{i\in\mathcal{I}}\sum_{k\in\mathcal{K}} \rho_{i,k}^{n,l} \geq 1, \forall n \in \mathcal{N}_x, x \in \{e,u\}, l \in \mathcal{L}, i \in \mathcal{I}, k \in \mathcal{K}$. Note that each user may be allocated at least one RB with the maximum allowable power for the worst throughput case.

$$\frac{\partial R_2^n(\widehat{\boldsymbol{P}})}{\partial \widehat{P}_{i,k}^{n,l}} = \begin{cases} \sum\limits_{\substack{k'=1, \left\lceil \frac{k'}{F_2} \right\rceil = \left\lceil \frac{k}{F_2} \right\rceil \\ (k' \bmod F_2) \neq (k \bmod F_2)}}^{K} \left(C_{1,k'}^1 C_{1,k'}^2 + C_{2,k'}^1 C_{k'}^4 \right) + C_{1,k}^1 C_1^3, \\ \qquad \text{if } i = 1, \\ \sum\limits_{\substack{k'=1, \left\lceil \frac{k'}{F_2} \right\rceil = \left\lceil \frac{k}{F_2} \right\rceil \\ (k' \bmod F_2) \neq (k \bmod F_2)}}^{K} \left(C_{2,k'}^1 C_{2,k'}^2 + C_{1,k'}^1 C_{k'}^5 \right) + C_{1,k}^1 C_2^3, \\ \qquad \text{if } i = 2, k \in \mathcal{F}_2, \\ \sum\limits_{\substack{k'=1, \left\lceil \frac{k'}{F_2} \right\rceil = \left\lceil \frac{k}{F_2} \right\rceil \\ (k' \bmod F_2) \neq (k \bmod F_2)}}^{K} \left(C_{2,k'}^1 C_{2,k'}^2 + C_{1,k'}^1 C_{k'}^6 \right) + C_{1,k}^1 C_2^3, \\ \qquad \text{if } i = 2, k \in \mathcal{K} \backslash \mathcal{F}_2 \end{cases} \tag{43}$$

$$C_{i',k'}^1 = \frac{T_{i'} \Delta f_{i'}}{\ln 2 \cdot \left(N_0 \Delta f_{i'} + \widehat{ICI}_{i',k'}^{l} + \widehat{ISI}_{i',k'}^{n,l} + \widehat{INI}_{\{\mathcal{I}\backslash i'\} \to i',k'}^{l} \right)},$$

$$C_{i',k'}^2 = \frac{\left| h_{i,k}^{n,l} \right|^2}{2(\Delta f_{i'})^2 \left[(k' \bmod F_{i'}) - (k \bmod F_{i'}) \right]^2} \cdot \left(\frac{f_c}{c} v_n \right)^2,$$

$$C_{i'}^3 = \left| h_{i,k}^{n,l} \right|^2 \Delta f_{i'} \int_0^{\xi_{\text{RMS}} - \frac{\gamma}{\Delta f_{i'}}} \int_{\frac{\gamma}{\Delta f_{i'}} + t}^{\xi_{\text{RMS}}} \Xi(\xi)\ d\xi dt,$$

$$C_{k'}^4 = \frac{\left| h_{i,k}^{n,l} \right|^2}{F_1 F_2} \left[\sum_{m \in \mathcal{M}} \left(\delta_{1 \to 2,m} \right)^{\sigma} \right]^{\frac{1}{\sigma}},$$

$$C_{k'}^5 = \frac{\left| h_{i,k}^{n,l} \right|^2}{F_1 F_2} \left[\sum_{m \in \mathcal{M}} \left(\delta_{2 \to 1,m}^{(1)} \right)^{\sigma} \right]^{\frac{1}{\sigma}},$$

$$C_{k'}^6 = \frac{\left| h_{i,k}^{n,l} \right|^2}{F_1 F_2} \left[\sum_{m \in \mathcal{M}} \left(\delta_{2 \to 1,m}^{(2)} \right)^{\sigma} \right]^{\frac{1}{\sigma}}$$

Algorithm 1: Proposed MNPRA Scheme

Initialize:
- Channel gain $h_{i,k}^{n,l}, \forall n \in \mathcal{N}, l \in \mathcal{L}, i \in \mathcal{I}, k \in \mathcal{K}$
- Iteration index of outer loop $j = 1$
- Allowable iteration upper bounds for inner/outer loops T_{in}/T_{out}
- Threshold of inner/outer convergence κ_{in}/κ_{out}
- Temporary EE parameter $\lambda[j]$
- Initialize random policy set $\{\boldsymbol{P}[j], \boldsymbol{\rho}[j], \boldsymbol{\alpha}[j]\}$ satisfying the conditions of $\min\ R^n(P_{\max}, \boldsymbol{\rho}, \boldsymbol{\alpha}) \geq R_{\min}^x$, $\max\ \Theta(l,i,k)\rho_{i,k}^{n,l} \leq \tau_x$, and $\sum_{l\in\mathcal{L}}\sum_{i\in\mathcal{I}}\sum_{k\in\mathcal{K}}\rho_{i,k}^{n,l} \geq 1$, $\forall n \in \mathcal{N}_x, x \in \{e,u\}, l \in \mathcal{L}, i \in \mathcal{I}, k \in \mathcal{K}$

repeat {EE Approximation}
- Calculate temporary EE parameter as $\lambda[j] = \frac{\sum_{n\in\mathcal{N}} R^n(\boldsymbol{P}[j],\boldsymbol{\rho}[j],\boldsymbol{\alpha}[j])}{\sum_{n\in\mathcal{N}}\sum_{l\in\mathcal{L}} P^{n,l}(\boldsymbol{P}[j],\boldsymbol{\rho}[j],\boldsymbol{\alpha}[j])}$
- Initialize iteration index of inner loop $j' = 1$
- **repeat** {Convex Problem Resolution}
  - Set temporary solution as $\{\widehat{\boldsymbol{P}}[j'], \widehat{\boldsymbol{\rho}}[j'], \widehat{\boldsymbol{\alpha}}[j']\} \leftarrow \{\boldsymbol{P}[j], \boldsymbol{\rho}[j], \boldsymbol{\alpha}[j]\}$
  - Calculate Taylor approximation of (46)
  - Solve convex problem $\mathcal{P}5$ in (47) given $\lambda[j]$
  - Obtain policy outcome as $\{\widehat{\boldsymbol{P}}[j'+1], \widehat{\boldsymbol{\rho}}[j'+1], \widehat{\boldsymbol{\alpha}}[j'+1]\}$
  - Increment of inner iteration index $j' \leftarrow j' + 1$
- **until** Satisfying (50) or $j' \geq T_{in}$
- Update $\{\boldsymbol{P}[j+1], \boldsymbol{\rho}[j+1], \boldsymbol{\alpha}[j+1]\} \leftarrow \{\widehat{\boldsymbol{P}}[j'], \widehat{\boldsymbol{\rho}}[j'], \widehat{\boldsymbol{\alpha}}[j']\}$
- Increment of outer iteration index $j \leftarrow j + 1$

until Satisfying (49) or $j \geq T_{out}$

Acquire the optimal solution $\{\boldsymbol{P}^*, \boldsymbol{\rho}^*, \boldsymbol{\alpha}^*\} = \{\boldsymbol{P}[j], \boldsymbol{\rho}[j], \boldsymbol{\alpha}[j]\}$ and corresponding EE performance $\Lambda(\boldsymbol{P}^*, \boldsymbol{\rho}^*, \boldsymbol{\alpha}^*)$

C. Convergence and Complexity Analysis

Since we convert the original fractional objective function to a subtractive D.C. form, we should prove that both iteration loops of Algorithm 1 will converge to its respective optimal candidate solutions.

Proposition 2: Improved solutions can be obtained from problem $\mathcal{P}2$ in (17)*, which results in a convergence of outer loop of MNPRA in Algorithm 1.*

Proof: First, we can infer from (17) *that the optimal EE obtained at j-th outer iteration is greater than zero, i.e.,*

$$\begin{aligned}
&\max_{\{\boldsymbol{P},\boldsymbol{\rho},\boldsymbol{\alpha}\}\in\mathcal{D}} \sum_{n\in\mathcal{N}} R^n(\boldsymbol{P},\boldsymbol{\rho},\boldsymbol{\alpha}) - \lambda[j] \\
&\quad\times\left(\sum_{n\in\mathcal{N}}\sum_{l\in\mathcal{L}} P^{n,l}(\boldsymbol{P},\boldsymbol{\rho},\boldsymbol{\alpha})\right) \\
&\geq \sum_{n\in\mathcal{N}} R^n(\boldsymbol{P}^*[j-1],\boldsymbol{\rho}^*[j-1],\boldsymbol{\alpha}^*[j-1]) \\
&\quad-\lambda[j]\left(\sum_{n\in\mathcal{N}}\sum_{l\in\mathcal{L}} P^{n,l}(\boldsymbol{P}^*[j-1],\boldsymbol{\rho}^*[j-1],\boldsymbol{\alpha}^*[j-1])\right) \\
&= 0. \qquad (51)
\end{aligned}$$

Note that $\lambda[j]$ is the optimal EE value obtained by the previous optimal solution set $\{\boldsymbol{P}^*[j-1], \boldsymbol{\rho}^*[j-1], \boldsymbol{\alpha}^*[j-1]\}$, i.e., $\lambda[j] = \frac{\sum_{n\in\mathcal{N}} R^n(\boldsymbol{P}^*[j-1],\boldsymbol{\rho}^*[j-1],\boldsymbol{\alpha}^*[j-1])}{\sum_{n\in\mathcal{N}}\sum_{l\in\mathcal{L}} P^{n,l}(\boldsymbol{P}^*[j-1],\boldsymbol{\rho}^*[j-1],\boldsymbol{\alpha}^*[j-1])}$. Substituting $\lambda[j]$ provokes the last equality in (51)*. Furthermore, we can rewrite*

$$\begin{aligned}
&\max_{\{\boldsymbol{P},\boldsymbol{\rho},\boldsymbol{\alpha}\}\in\mathcal{D}} \sum_{n\in\mathcal{N}} R^n(\boldsymbol{P},\boldsymbol{\rho},\boldsymbol{\alpha}) - \lambda[j] \\
&\quad\times\left(\sum_{n\in\mathcal{N}}\sum_{l\in\mathcal{L}} P^{n,l}(\boldsymbol{P},\boldsymbol{\rho},\boldsymbol{\alpha})\right) \\
&= \sum_{n\in\mathcal{N}} R^n(\boldsymbol{P}^*[j],\boldsymbol{\rho}^*[j],\boldsymbol{\alpha}^*[j]) \qquad (52) \\
&\quad-\lambda[j]\left(\sum_{n\in\mathcal{N}}\sum_{l\in\mathcal{L}} P^{n,l}(\boldsymbol{P}^*[j],\boldsymbol{\rho}^*[j],\boldsymbol{\alpha}^*[j])\right) \\
&= \lambda[j+1]\left(\sum_{n\in\mathcal{N}}\sum_{l\in\mathcal{L}} P^{n,l}(\boldsymbol{P}^*[j],\boldsymbol{\rho}^*[j],\boldsymbol{\alpha}^*[j])\right) \qquad (53) \\
&\quad-\lambda[j]\left(\sum_{n\in\mathcal{N}}\sum_{l\in\mathcal{L}} P^{n,l}(\boldsymbol{P}^*[j],\boldsymbol{\rho}^*[j],\boldsymbol{\alpha}^*[j])\right) \geq 0. \qquad (54)
\end{aligned}$$

The last inequality holds due to the derivation from (51)*. Therefore, we can conclude that $\lambda[j+1] \geq \lambda[j], \forall j$. We can deduce that the solution of outer loop of MNPRA in Algorithm 1 will be improved until convergence. This completes the proof.* □

Proposition 3: The solution obtained by problem $\mathcal{P}5$ in (47) *corresponding to the inner loop of MNPRA in Algorithm 1 will converge to a local optimum.*

Proof: We adopt a similar derivation manner in Proposition 2 to prove inner loop of MNPRA to converge. Owing to the concave function of $F_2(\widehat{\boldsymbol{P}}, \widehat{\boldsymbol{\rho}}, \widehat{\boldsymbol{\alpha}})$, it can be inferred that the first-order Taylor approximation of $F(\widehat{\boldsymbol{P}}, \widehat{\boldsymbol{\rho}}, \widehat{\boldsymbol{\alpha}})$ becomes the lower bound of its original function. Then, we have the following deduction in the inner loop of Algorithm 1, shown at the bottom of the next page. Note that $\mathcal{D}''$ is defined as a feasible set containing all constraints in $\mathcal{P}5$. Based on the relationship stated above, we conclude that the optimal value of $\mathcal{P}5$ in (47) *will be improved or stay unchanged. When $j' \to \infty$, we can acquire the optimum by $\{\widehat{\boldsymbol{P}}^*, \widehat{\boldsymbol{\rho}}^*, \widehat{\boldsymbol{\alpha}}^*\} = \lim_{j\to\infty} F(\widehat{\boldsymbol{P}}[j'], \widehat{\boldsymbol{\rho}}[j'], \widehat{\boldsymbol{\alpha}}[j'])$. That is, the solution obtained by problem $\mathcal{P}5$ in* (47) *in the inner loop of MNPRA in Algorithm 1 will converge to a local optimum. This completes the proof.* □

Moreover, we compare the computational complexity of proposed MNPRA with the global solution. For an MN system with I numerologies, K RBs, and N users, the computational complexity of obtaining the global optimum is $\mathcal{O}\left((|\boldsymbol{P}|\cdot 2)^{L\cdot(IKN+M)}\right)$, which is not implementable due to its exponential complexity. Note that $|\boldsymbol{P}|$ is the searching space over power assignment. Based on algorithm 1, the proposed MNPRA scheme has a complexity order of $\mathcal{O}(|\widehat{\boldsymbol{P}}|\cdot|\widehat{\boldsymbol{\rho}}|\cdot|\widehat{\boldsymbol{\alpha}}|)$ with the relaxed continuous solution set size of RB $|\widehat{\boldsymbol{\rho}}|$ and of NBR $|\widehat{\boldsymbol{\alpha}}|$. It can be inferred that $|\widehat{\boldsymbol{P}}| = |\boldsymbol{P}|$, $|\widehat{\boldsymbol{\rho}}| \ll 2^{LIKN}$, and $|\widehat{\boldsymbol{\alpha}}| \ll 2^{LM}$ based on convex optimization operation, which achieves a considerably lower and implementable complexity order than that of global optimum.

IV. Performance Evaluation

We evaluate the system performance of proposed MNPRA scheme via simulations. We consider the total bandwidth

TABLE I
PARAMETER SETTING

System Parameters	Symbol	Value
System total bandwidth	BW	180 kHz
System carrier frequency	f_c	3.5 GHz
Number of numerologies	I	2
Number of sub-RGs	L	3
Number of RBs	K	12
Number of users	(N_e, N_u)	$(4, 4)$
SCS of numerology	Δf_i	$(15, 30, 60)$ kHz
CP ratio of ISI	γ	0.07
Channel RMS delay	ξ_{RMS}	28 μs
Average velocity of users	v_n	60 km/hr
Velocity perturbation	-	5% of its average
Noise power spectral density	N_0	-174 dBm/Hz
Power amplifier efficiency	η_{PA}	5
Circuit power over sub-RG	P_{circuit}	10 dBm
Maximum per-RB power	$P_{\max}$	20 dBm
Maximum total transmit power	$P_{\max}^{\text{tot}}$	30 dBm
QoS requirement	$(R_{\min}^{e}, R_{\min}^{u})$	$(500, 100)$ bits
Delay restrictions	(τ_e, τ_u)	$(3, 1)$ ms
Penalty of integer relaxation	$(\beta_\rho, \beta_\alpha)$	$(10^6, 10^2)$
Iteration upper bound	(T_{in}, T_{out})	$(100, 30)$
Difference threshold	$(\kappa_{in}, \kappa_{out})$	$(0.1, 0.1)$ bits/J
Monte Carlo runs	-	100
Timeslot per run	-	100

and time duration of MN configurations as 180 kHz and 2 ms, respectively. The two of three selected numerologies are adopted in our simulation, including numerology-1 with $s_1 = 0$, $\Delta f_1 = 15$ kHz, $T_1 = 1$ ms, $F_1 = 12$ sub-carriers, numerology-2 with $s_2 = 1$, $\Delta f_2 = 30$ kHz, $T_2 = 0.5$ ms, $F_2 = 6$ sub-carriers, and numerology-3 with $s_3 = 2$, $\Delta f_2 = 60$ kHz, $T_3 = 0.25$ ms, $F_3 = 3$ sub-carriers. Note that all numerologies possess the totally identical bandwidth for fair comparison. We consider that the channel experiences a small-scale Rayleigh fading with complex Gaussian distribution as $h_{i,k}^{n,l} \sim \mathcal{CN}(0, 1)$. The CP ratio of ISI is set as $\gamma = 0.07$, whilst RMS delay is $\xi_{\text{RMS}} = 28$ μs. We notice that throughput is calculated based on the multiplication of bandwidth, time duration and signal strength resulting in a unit of bits, whilst energy is in a unit of J, namely Joule. Note that all users are supposed to have the same velocity. To average the channel variations, the simulations are performed over around 100 Monte Carlo iterations with 100 timeslots per Monte Carlo run. We consider that the BS is capable of periodically collecting user velocity information from the receiver ends with second-level, which is much longer than channel coherence time with milliseconds. Accordingly, the velocity is regarded as a constant under the execution of resource allocation. Nevertheless, due to mechanical perturbation on device, we consider the velocity variance with 5% of its average value. For example, user with average speed of 60 km/hr possesses a velocity range of $[57, 63]$ km/hr. For simplicity, we only label the average velocity values in the simulations. The remaining parameter setting referring [17], [47] is summarized in Table I.

A. Convergence of MNPRA

We firstly evaluate the convergence of proposed MNPRA scheme under TD-MN and FD-MN for outer and inner parts of EE optimization. Note that the Dinkelbach value in the outer iteration is referring (18). We can observe from Figs. 4(a) and 4(b) that the FD-MN requires more iterations for converging its optimal solution due to more flexible numerology structure simultaneously benefiting all services, whereas TD-MN having quicker convergence owing to a single transmission type at a single timeslot. Furthermore, it is observed that the proposed scheme asymptotically approaches the global optimum in Dinkelbach values with corresponding EE difference lower than 0.2×10^6 bits/J. As seen in Fig. 4(b), FD-MN requires more iteration rounds as well as higher computational complexity order to conduct resource allocation due to severe INI effect. Moreover, following the same reason, TD-MN may achieve higher EE performance than FD-MN, i.e., at an EE difference of around 10^6 bits/J, which strikes a compelling tradeoff between the flexibility of resource allocation and convergence performance.

B. Impacts of INI

We reveal an example for the impact of ICI and INI in frequency-domain as demonstrated in Fig. 5. Note that similar figure can be shown for ISI in time-domain, which is neglected here because of it compellingly smaller influence. We consider three exemplified signal sources, including signal with SCS of 15 kHz and that with Doppler effect as well as the one

$$
\begin{aligned}
F(\widehat{\boldsymbol{P}}[j'], \widehat{\boldsymbol{\rho}}[j'], \widehat{\boldsymbol{\alpha}}[j']) &= F_1(\widehat{\boldsymbol{P}}[j'], \widehat{\boldsymbol{\rho}}[j'], \widehat{\boldsymbol{\alpha}}[j']) - F_2(\widehat{\boldsymbol{P}}[j'], \widehat{\boldsymbol{\rho}}[j'], \widehat{\boldsymbol{\alpha}}[j']) \\
&\geq F_1(\widehat{\boldsymbol{P}}[j'], \widehat{\boldsymbol{\rho}}[j'], \widehat{\boldsymbol{\alpha}}[j']) - F_2(\widehat{\boldsymbol{P}}[j'-1], \widehat{\boldsymbol{\rho}}[j'-1], \widehat{\boldsymbol{\alpha}}[j'-1]) \\
&\quad - \sum_{\boldsymbol{X} \in \{\widehat{\boldsymbol{P}}, \widehat{\boldsymbol{\rho}}, \widehat{\boldsymbol{\alpha}}\}} \nabla_{\boldsymbol{X}}^T F_2(\widehat{\boldsymbol{P}}[j'-1], \widehat{\boldsymbol{\rho}}[j'-1], \widehat{\boldsymbol{\alpha}}[j'-1]) \cdot \Big(\boldsymbol{X}[j'] - \boldsymbol{X}[j'-1]\Big) \\
&= \max_{\{\widehat{\boldsymbol{P}}, \widehat{\boldsymbol{\rho}}, \widehat{\boldsymbol{\alpha}}\} \in \mathcal{D}''} F_1(\widehat{\boldsymbol{P}}, \widehat{\boldsymbol{\rho}}, \widehat{\boldsymbol{\alpha}}) - F_2(\widehat{\boldsymbol{P}}[j'-1], \widehat{\boldsymbol{\rho}}[j'-1], \widehat{\boldsymbol{\alpha}}[j'-1]) \\
&\quad - \sum_{\boldsymbol{X} \in \{\widehat{\boldsymbol{P}}, \widehat{\boldsymbol{\rho}}, \widehat{\boldsymbol{\alpha}}\}} \nabla_{\boldsymbol{X}}^T F_2(\widehat{\boldsymbol{P}}[j'-1], \widehat{\boldsymbol{\rho}}[j'-1], \widehat{\boldsymbol{\alpha}}[j'-1]) \cdot \Big(\boldsymbol{X} - \boldsymbol{X}[j'-1]\Big) \\
&\geq F_1(\widehat{\boldsymbol{P}}[j'-1], \widehat{\boldsymbol{\rho}}[j'-1], \widehat{\boldsymbol{\alpha}}[j'-1]) - F_2(\widehat{\boldsymbol{P}}[j'-1], \widehat{\boldsymbol{\rho}}[j'-1], \widehat{\boldsymbol{\alpha}}[j'-1]) \\
&\quad - \sum_{\boldsymbol{X} \in \{\widehat{\boldsymbol{P}}, \widehat{\boldsymbol{\rho}}, \widehat{\boldsymbol{\alpha}}\}} \nabla_{\boldsymbol{X}}^T F_2(\widehat{\boldsymbol{P}}[j'-1], \widehat{\boldsymbol{\rho}}[j'-1], \widehat{\boldsymbol{\alpha}}[j'-1]) \cdot \Big(\boldsymbol{X}[j'-1] - \boldsymbol{X}[j'-1]\Big) \\
&= F(\widehat{\boldsymbol{P}}[j'-1], \widehat{\boldsymbol{\rho}}[j'-1], \widehat{\boldsymbol{\alpha}}[j'-1])
\end{aligned} \tag{55}
$$

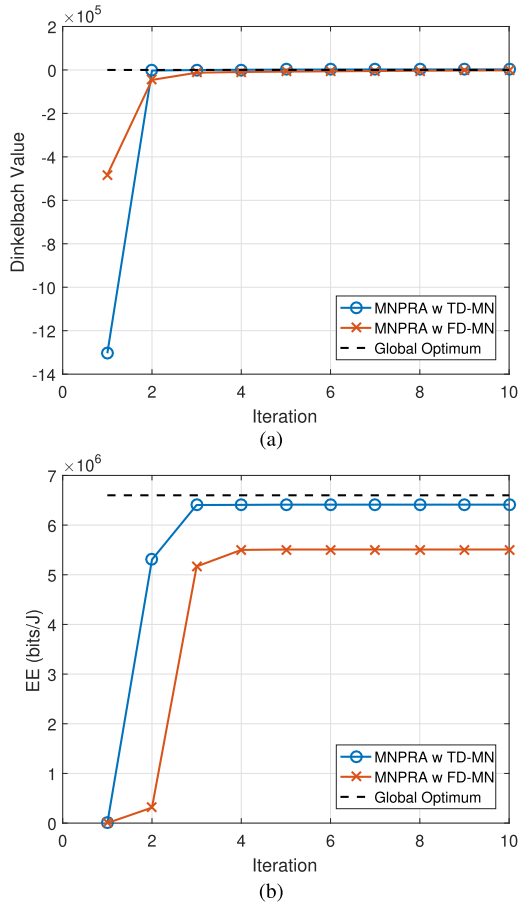

Fig. 4. Convergence of proposed MNPRA scheme under TD-MN and FD-MN for (a) outer iteration of EE approximation and (b) inner iteration of EE problem resolution.

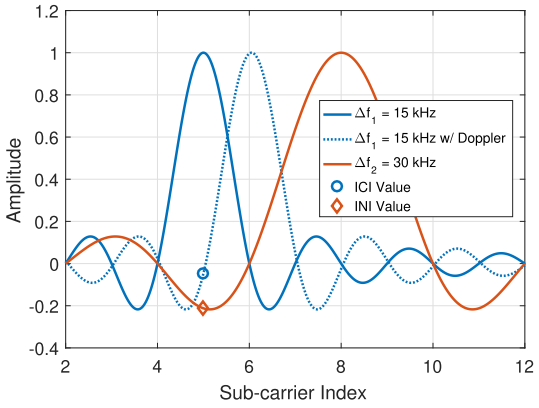

Fig. 5. Illustration of ICI and INI.

of 30 kHz. As explained previously, Doppler effect will cause ICI, whilst different numerologies provoke INI between each other. As observed from the figure, the ICI-induced signal leads to a smaller degradation than INI. This is because that different numerologies have totally alternated from their original orthogonal waveforms to non-orthogonal ones.

Moreover, in Fig. 6, we characterize the INI power and its upper bound as demonstrated in Lemma 1 by considering fixed numerology's NBR $\eta \in \{\frac{1}{6}, \frac{2}{6}, \frac{3}{6}, \frac{4}{6}\}$ and parameter

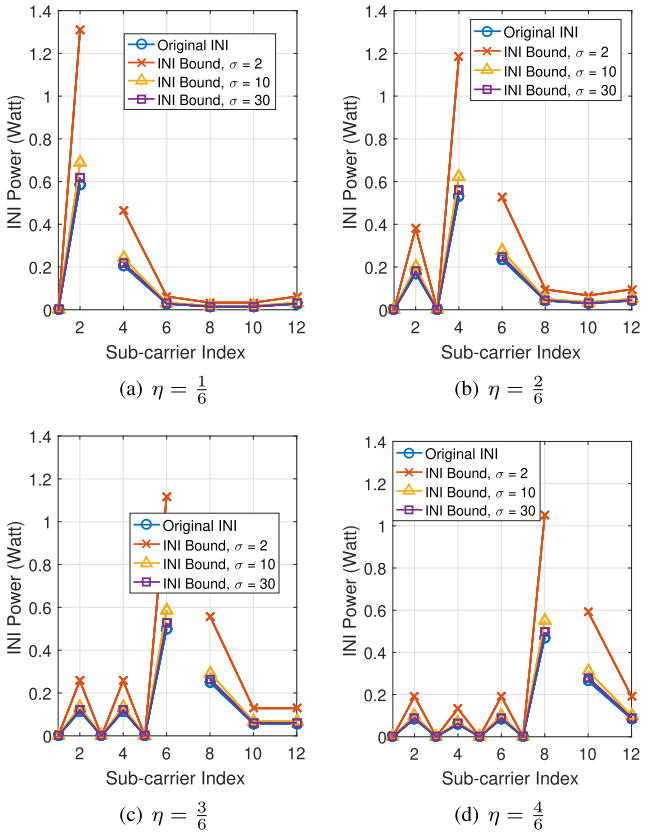

Fig. 6. Comparison between original INI power and INI upper bounds under different configurations of NBR $\eta \in \{\frac{1}{6}, \frac{2}{6}, \frac{3}{6}, \frac{4}{6}\}$ and INI upper bound parameter $\sigma \in \{2, 10, 30\}$.

of $\sigma \in \{2, 10, 30\}$. Note that power is equally assigned to all sub-carriers for readily observing effect of INI before resource allocation. Note that we select numerology-1 occupying the RBs with sub-carriers indexed from 1 to ηF_1, whilst numerology-2 utilizes the remaining sub-carriers. Accordingly, the INI at the left-hand side of each subfigure is termed as interference generated from numerology-2 and received by numerology-1, and vice versa for the other side. We can observe that the boundary sub-carriers suffer from considerable INI degradation, for example, the 2-nd as well as 4-th sub-carriers in Fig. 6(a) have the highest INI peaks in their respective numerology configuration. Furthermore, the remote sub-carriers will receive less INI due to adequately weak sidelobes. We can infer from Figs. 6(b) to 6(d) that INI generated by numerology-2 periodically fluctuates owing to discontinuous concatenation of its symbols with twice bandwidth compared to numerology-1. Therefore, we should assign appropriate power and RBs for mitigating such condition. With the increment of η, lower INI from numerology-2 can be acquired, whereas higher interference from numerology-1 occurs due to more allocated resources to that configuration. Moreover, with the aid of higher value of σ, a tighter bound of INI can be achieved and consequently $\sigma = 30$ is selected in our following simulation setting.

The resultant INI of proposed MNPRA scheme is shown in Fig. 7 by considering two numerologies and fixed NBR $\eta = \{\frac{1}{6}, \frac{2}{6}\}$, where Fig. 7(a) and Fig. 7(b) have demonstrated

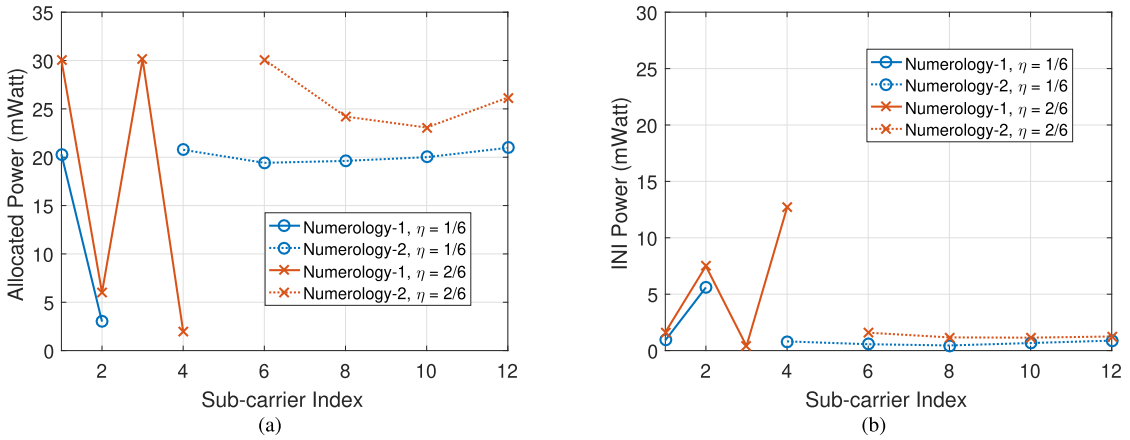

Fig. 7. The resultant power of the proposed MNPRA scheme in terms of (a) allocated power and (b) corresponding INI power on different sub-carriers with two numerologies and $\eta \in \{\frac{1}{6}, \frac{2}{6}\}$.

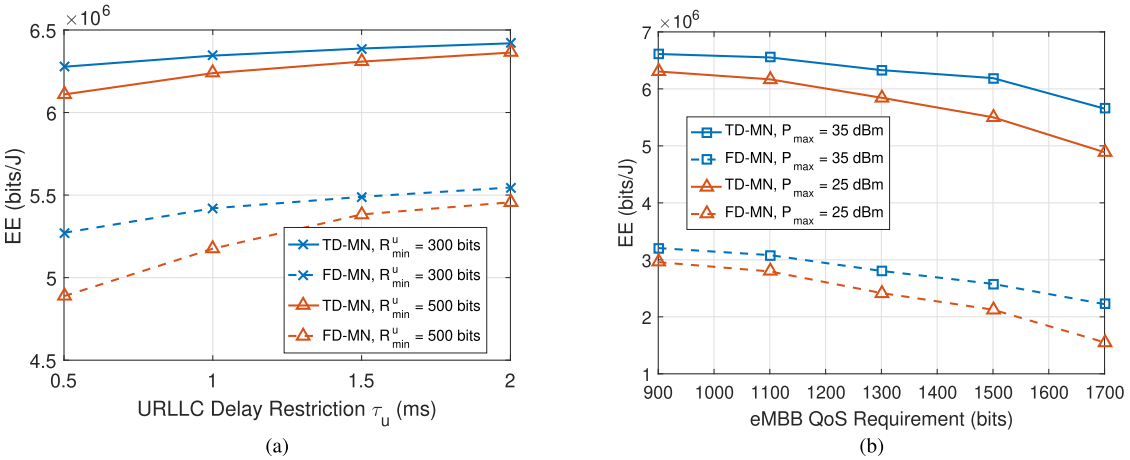

Fig. 8. Performance of the proposed MNPRA algorithm using TD-/FD-MN under different services constrained by (a) delay restriction and (b) QoS requirement.

the assigned power and the corresponding INI values, respectively. We can know that lower INI can be achieved with the benefit of lower power assigned. By contrast, more power can be allocated to those sub-carriers with little interference for improving rate performance. Moreover, when $\eta = \frac{2}{6}$, more power is required to mitigate interference, as observed by comparing Figs. 6(b) and 7(a), which results in comparably smaller INI in Fig. 7(b), i.e., the original non-optimized INI of around 600 mWatt is reduced to around 13 mWatt at sub-carrier 4 under MNPRA. However, fixed numerology is potentially unable to meet the requirement for complex use cases of multi-service optimization, which will be discussed in the following simulations.

C. Effect of Service Constraints

In Fig. 8, we have studied the EE performance of proposed MNPRA algorithm under TD-/FD-MN constrained by different service requirements. As shown in Fig. 8(a), we can observe an increased EE curve with looser delay constraint for URLLC services owing to more flexible numerology assignment. Moreover, FD-MN inducing severe INI leads to a comparably lower EE due to simultaneous satisfaction of both URLLC and eMBB services, especially when restricted by higher QoS demands, which can also be found in Fig. 8(b). Additionally, little performance difference can be reached under relaxed requirements of delay and QoS in both results, i.e., we have an EE difference from 5×10^5 to 10^5 bits/J in FD-MN from $\tau_u = 0.5$ to 2 ms, as seen in Fig. 8(a). To elaborate on a little further, we observe from Fig. 8(b) that higher EE is attained if more power is utilized to flexibly and properly assign radio resources for alleviating interferences of ICI, ISI and INI, i.e., it improves EE of around 5×10^5 bits/J by increasing power from 25 to 35 dBm.

D. Impact of User Velocity

We evaluate the performance of user velocity on EE performance of proposed MNPRA scheme considering different channel delay spread $\tau_{\text{RMS}} \in \{2, 28\}$ μs under TD-/FD-MN in Fig. 9. Note that we fix $\Delta f_1 = 15$ kHz and adjust different $\Delta f_2 \in \{30, 60\}$ kHz, i.e., $Q = \frac{\Delta f_2}{\Delta f_1}$ to observe the effect of different numerology's setting. Note that $Q = 1$ is for TD-MN adopting one type of the two numerologies $\{\Delta f_1, \Delta f_2\}$ in each RBG. We can readily observe that EE performance monotonically decreases with the increment of velocity values

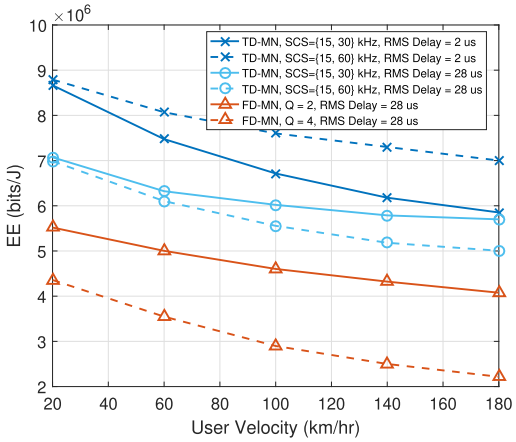

Fig. 9. The EE performance versus user velocity $v_n \in [20, 180]$ km/hr under different RMS delay spread $\tau_{\text{RMS}} \in \{2, 28\}$ μs and numerology configuration of $Q = \Delta f_2/\Delta f_1 \in \{2, 4\}$. Note that $Q = 1$ is for TD-MN adopting one type of the two numerologies in each RBG.

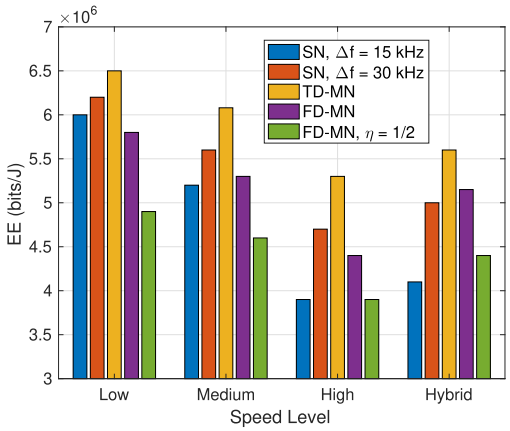

Fig. 10. EE versus scenario employing different schemes.

owing to severe ICI caused by the Doppler shift. Moreover, we can see that the channel experiencing a longer delay spread leads to a degradation of EE performance due to the ISI. It has a better EE of $Q = 4$ than that of $Q = 2$ when it experiences low RMS delay spread of 2 μs, which is mainly caused by lower ICI from wider bandwidth as observed from (4). However, it performs reversely under high delay spread of 28 μs thanks to simultaneous mitigation of both ICI and ISI. That is, selection of a smaller SCS $Q = 2$ is capable of resolving comparably severe ISI problem in higher delay spread than that in a lower one. Furthermore, when increasing user speed, EE difference becomes remarkably larger from $Q = 2$ to $Q = 4$ mainly due to high ICI generated by large SCS. To elaborate a little further, we compare TD-MN and FD-MN under delay spread of 28 μs. It is revealed that lower EE is obtained when configured with FD-MN compared to that with TD-MN, which is substantially affected by relentless INI, i.e., we observe an EE difference of about 1.5×10^6 bits/J when SCS as $\{15, 30\}$ kHz and around 2.8×10^6 bits/J when SCS as $\{15, 60\}$ kHz under most of user velocities. Such high EE difference is mainly caused by high SCS since SCS with 60 kHz in SCS set of $\{15, 60\}$ kHz causes larger INI than that with SCS set of $\{15, 30\}$ kHz spacing.

E. Comparison Between SN/MN Under Different Scenarios

As depicted in Fig. 10, we evaluate the performance of proposed MNPRA scheme under TD-/FD-MN by comparing SN and fixed MN. Different scenarios are considered, including low, medium and high as well as hybrid speed levels, which represent user velocity of 20, 60, 200 and a hybrid case of $\{20, 200\}$ km/hr, respectively. Note that one of $\{15, 30\}$ kHz is adopted as SCS in SN, whilst $\Delta f_1 = 15$ kHz is set in MN. We know that large SCS is applicable for ICI-dominated channels, whereas small SCS benefits ISI-based environments. Therefore, similar observation can be readily inferred from both Figs. 9 and 10 that TD-MN outperforms the other mechanisms in support of flexible assignment of different numerologies. Nevertheless, FD-MN is compromising its EE for providing hybrid services, which is mainly degraded by INI effect. Moreover, FD-MN with fixed NBR $\eta = \frac{1}{2}$ admits the worst performance due to inflexibility of RB assignment for different services, which induces even higher INI than flexible NBR selection, i.e., around 10^6 bits/J degradation compared to dynamic NBR allocation. Additionally, under a hybrid-speed scenario, MNPRA under TD-/FD-MN is able to deal with all interferences by striking a tradeoff between performance and different service requirements.

In order to reveal its benefits of FD-MN in our proposed MNPRA, we further evaluate the scenario with different ratios of URLLC users to all serving users as $\{25, 50, 75\}\%$. Note that outage is calculated if the outcome does not satisfy either constraints (15b) and (15d) for eMBB service or (15c) and (15e) for URLLC users. We can observe that under fewer URLLC users, i.e., at a ratio of $\{25, 50\}\%$, MNPRA in TD-MN attains the highest EE in Fig. 11(a) with an acceptably lower outage probability in Figs. 11(b) and 11(c), which is benefited by moderate assignment of RB and power. Nonetheless, EE of SN configuration becomes inadequate by considerably downgrading the outage performance owing to little degree of freedom for flexible allocation, i.e., SN with SCS of 15 kHz leads to around 0.25 throughput outage and 0.09 delay outage under a ratio of 25% URLLC users. We now turn to the results of FD-MN, which outperforms the other mechanisms when 75% URLLC users are served. This is because FD-MN allows the co-existence of multiple numerologies within a single timeslot, supporting simultaneous throughput- and delay-oriented applications while mitigating induced interferences. FD-MN offering resilient services performs a even lower outage below 0.05 than the other configurations with respect to both throughput and delay outage probabilities.

F. Benchmark Comparison of MNPRA

In Fig. 12, we compare the proposed MNPRA scheme to the existing four benchmarks (BMs) in open literature and the baseline as elaborated as follows.

- **BM1: Sliding Window** [17] utilizes a fixed-size temporal sliding window to gradually assign MN-based RBs to mainly fulfill latency-aware applications. The power is assigned to meet the essential requirement of rate-oriented users. Note that the channel fluctuation is not

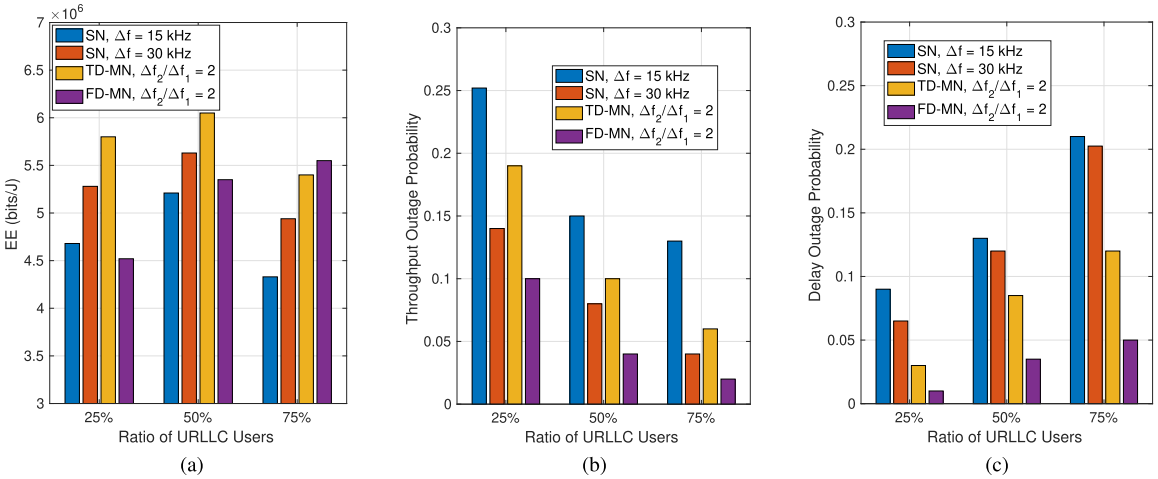

Fig. 11. Comparison of SN, TD-/FD-MN considering different ratios of URLLC users as $\{25, 50, 75\}\%$ in terms of (a) EE (b) throughput outage and (c) delay outage.

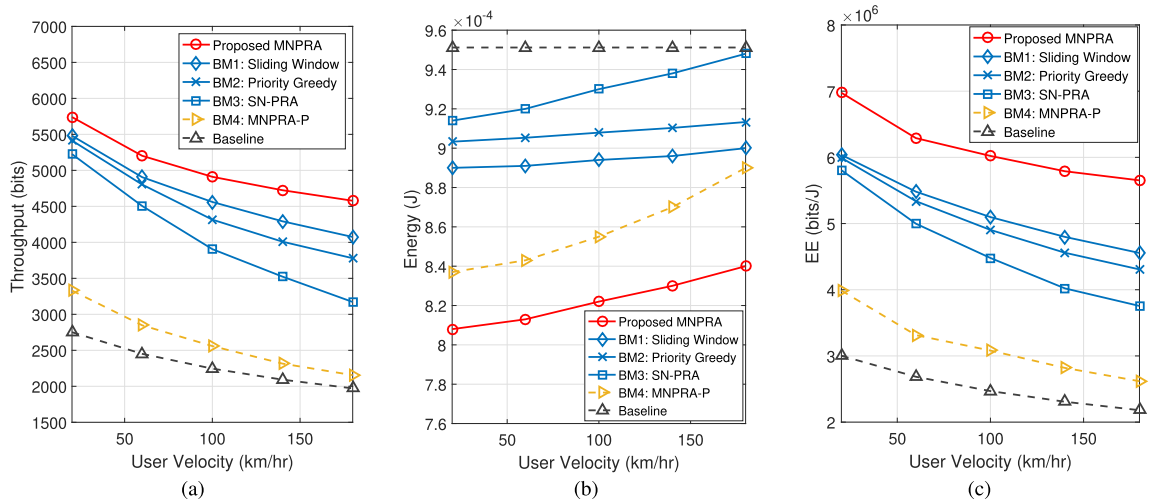

Fig. 12. Comparison between proposed MNPRA algorithm and other baselines. (a) EE versus user velocity v_n (b) Throughput versus user velocity v_n (c) Energy versus user velocity v_n.

considered, that is, all RBs are considered to possess the same channel condition.

- **BM2: Priority Greedy** [21] performs MN-enabled resource allocation according to a priority-based greedy method and queuing conditions. This method assigns low-delay based numerology's resources to the time-critical tasks. The power is allocated to meet the QoS constraint.
- **BM3: SN-PRA** [47] conducts EE-based power-RB allocation under conventional SN structure. The problem is resolved based on D.C. transformation as well as integer relaxation for tackling binary variables. However, it induces quantization errors when converting from the continuous relaxed RB indicator to the discrete one.
- **BM4: MNPRA-P** employs solely power allocation scheme in Algorithm 1 under MN, whereas RB is arbitrarily assigned. Note that we would like to observe the improvement of either sub-carrier or power assignment.
- **Baseline** adopts a round robin method to randomly allocate RBs in an MN-enabled system, whilst the power is equally assigned constrained by its allowable maximum transmit power.

We can know from Figs. 12(a) and 12(b) that BM3 using SN-based system experiences a stringent service under inflexible frame structure, which results in a comparably lower throughput and higher consumed energy than BMs 1 and 2 in an MN-enabled network. Following the same reason, the difference of the required energy in SN-PRA is higher than BMs 1 and 2 owing to its fixed framing. Moreover, BM1 reaches a better performance than BM2. This is because BM1 performs local optimization by sliding with a window size, whilst priority based method will relentlessly sacrifice the other user demands for supporting a more urgent task. To elaborate a little further, as shown in Fig. 12(c), it reveals a compelling performance gap in EE if improper RB policy is conducted in an MN system, i.e., BM4 has an EE degradation of around 30% and 45% compared to BMs 1 and 2 as well as the proposed MNPRA scheme, respectively. Moreover, we can achieve at least 15% improvement under the optimal power allocation, i.e., MNPRA attains an enhanced EE compared to BMs 1 and 2 from 6×10^6 to 7×10^6 bits/J under the lowest velocity. In this context, we can summarize from Figs. 12(a) and 12(b) that the proposed MNPRA achieves the highest throughput and consumes the lowest energy since

it appropriately assigns RBs and power to conquer serious impacts of INI, ISI, and ICI. As illustrated in Fig. 12(c), MNPRA also results in the highest EE comparing to other existing methods in open literature.

V. Conclusion

In this paper, we have conceived an MNPRA scheme to resolve the designed EE optimization under a mobility-aware MN network. We have also characterized the temporal and spectral interferences of ICI, ISI and INI in MN. The non-solvable problem is transformed into a convex and solvable one with the benefit of Dinkelbach process, D.C. approximation and advanced integer relaxation. The local convergence of MNPRA is proven and validated through theory and simulation. We can observe that the proposed MNPRA can strike a compelling tradeoff between EE improvement and throughput/delay satisfaction under different parameter setting. Benefited by flexible numerology and resource allocation, the proposed MNPRA achieves the highest EE and throughput performance as well as the lowest consumed energy compared to the other existing benchmarks in open literature.

References

[1] A. A. Zaidi, R. Baldemair, V. Moles-Cases, N. He, K. Werner, and A. Cedergren, "OFDM numerology design for 5G new radio to support IoT, eMBB, and MBSFN," *IEEE Commun. Standards Mag.*, vol. 2, no. 2, pp. 78–83, Jun. 2018.

[2] Z. E. Ankarali, B. Peköz, and H. Arslan, "Flexible radio access beyond 5G: A future projection on waveform, numerology, and frame design principles," *IEEE Access*, vol. 5, pp. 18295–18309, 2017.

[3] Z. Zhang *et al.*, "6G wireless networks: Vision, requirements, architecture, and key technologies," *IEEE Veh. Technol. Mag.*, vol. 14, no. 3, pp. 28–41, Sep. 2019.

[4] L. Marijanovic, S. Schwarz, and M. Rupp, "Multiplexing services in 5G and beyond: Optimal resource allocation based on mixed numerology and mini-slots," *IEEE Access*, vol. 8, pp. 209537–209555, 2020.

[5] J. Mao, L. Zhang, P. Xiao, and K. Nikitopoulos, "Interference analysis and power allocation in the presence of mixed numerologies," *IEEE Trans. Wireless Commun.*, vol. 19, no. 8, pp. 5188–5203, Aug. 2020.

[6] S. Samarakoon, M. Bennis, W. Saad, and M. Debbah, "Distributed federated learning for ultra-reliable low-latency vehicular communications," *IEEE Trans. Commun.*, vol. 68, no. 2, pp. 1146–1159, Nov. 2020.

[7] G. Pocovi, K. I. Pedersen, B. Soret, M. Lauridsen, and P. Mogensen, "On the impact of multi-user traffic dynamics on low latency communications," in *Proc. Int. Symp. Wireless Commun. Syst. (ISWCS)*, Sep. 2016, pp. 204–208.

[8] G. Durisi, T. Koch, and P. Popovski, "Toward massive, ultrareliable, and low-latency wireless communication with short packets," *Proc. IEEE*, vol. 104, no. 9, pp. 1711–1726, Aug. 2016.

[9] W. R. Ghanem, V. Jamali, Y. Sun, and R. Schober, "Resource allocation for multi-user downlink MISO OFDMA-URLLC systems," *IEEE Trans. Commun.*, vol. 68, no. 11, pp. 7184–7200, Nov. 2020.

[10] N. Li, Z. Yao, Y. Tu, and Y. Chen, "Cooperative optimization for OFDMA resource allocation in multi-RRH millimeter-wave CRAN," *IEEE Access*, vol. 8, pp. 164035–164044, 2020.

[11] P.-Y. Wu, L.-H. Shen, and K.-T. Feng, "Virtual user emulation and resource allocation designs for 5G mobile wireless networks," in *Proc. IEEE Global Commun. Conf. (GLOBECOM)*, Dec. 2021, pp. 1–6.

[12] Y.-T. Huang, C.-H. Fang, L.-H. Shen, and K.-T. Feng, "Optimal functional split for processing sharing based CoMP for mixed eMBB and uRLLC traffic," in *Proc. IEEE Global Commun. Conf. (GLOBECOM)*, Dec. 2020, pp. 1–6.

[13] F. Raphel and S. Sameer, "A speed adaptive joint subcarrier and power allocation technique for downlink OFDMA video transmission over doubly selective channels," *IEEE Trans. Veh. Technol.*, vol. 69, no. 2, pp. 1879–1887, Feb. 2020.

[14] J. Jang and H. J. Yang, "Deep reinforcement learning-based resource allocation and power control in small cells with limited information exchange," *IEEE Trans. Veh. Technol.*, vol. 69, no. 11, pp. 13768–13783, Nov. 2020.

[15] L. Ferdouse, I. Woungang, A. Anpalagan, and S. Erkucuk, "Energy efficient downlink resource allocation in cellular IoT supported H-CRANs," *IEEE Trans. Veh. Technol.*, vol. 70, no. 6, pp. 5803–5816, Jun. 2021.

[16] T. T. Nguyen, V. N. Ha, and L. B. Le, "Wireless scheduling for heterogeneous services with mixed numerology in 5G wireless networks," *IEEE Commun. Lett.*, vol. 24, no. 2, pp. 410–413, Feb. 2020.

[17] W. Sui, X. Chen, S. Zhang, Z. Jiang, and S. Xu, "Energy-efficient resource allocation with flexible frame structure for hybrid eMBB and URLLC services," *IEEE Trans. Green Commun. Netw.*, vol. 5, no. 1, pp. 72–83, Mar. 2021.

[18] P. K. Korrai, E. Lagunas, A. Bandi, S. K. Sharma, and S. Chatzinotas, "Joint power and resource block allocation for mixed-numerology-based 5G downlink under imperfect CSI," *IEEE Open J. Commun. Soc.*, vol. 1, pp. 1583–1601, 2020.

[19] X. Zhang, L. Zhang, P. Xiao, D. Ma, J. Wei, and Y. Xin, "Mixed numerologies interference analysis and inter-numerology interference cancellation for windowed OFDM systems," *IEEE Trans. Veh. Tech.*, vol. 67, no. 8, pp. 7047–7061, Apr. 2018.

[20] A. B. Kihero, M. S. J. Solaija, and H. Arslan, "Inter-numerology interference for beyond 5G," *IEEE Access*, vol. 7, pp. 146512–146523, 2019.

[21] T. Bag, S. Garg, Z. Shaik, and A. Mitschele-Thiel, "Multi-numerology based resource allocation for reducing average scheduling latencies for 5G NR wireless networks," in *Proc. Eur. Conf. Netw. Commun. (EuCNC)*, Jun. 2019, pp. 597–602.

[22] A. Yazar and H. Arslan, "Reliability enhancement in multi-numerology-based 5G new radio using INI-aware scheduling," *EURASIP J. Wireless Commun. Netw.*, vol. 2019, no. 1, p. 110, Dec. 2019.

[23] C.-Y. Su, C.-H. Fang, L.-H. Shen, and K.-T. Feng, "Effective capacity maximization for multi-numerology based 5G NR networks," in *Proc. IEEE 92nd Veh. Technol. Conf. (VTC-Fall)*, Nov. 2020, pp. 1–5.

[24] L. Liang, H. Ye, G. Yu, and G. Y. Li, "Deep-learning-based wireless resource allocation with application to vehicular networks," *Proc. IEEE*, vol. 108, no. 2, pp. 341–356, Feb. 2020.

[25] X. Liu, M. Chen, Y. Liu, Y. Chen, S. Cui, and L. Hanzo, "Artificial intelligence aided next-generation networks relying on UAVs," *IEEE Wireless Commun.*, vol. 28, no. 1, pp. 120–127, Feb. 2021.

[26] B. Ai, A. F. Molisch, M. Rupp, and Z. D. Zhong, "5G key technologies for smart railways," *Proc. IEEE*, vol. 108, no. 6, pp. 856–893, Jun. 2020.

[27] V. Stoynov, D. Mihaylova, Z. Valkova-Jarvis, G. Iliev, and V. Poulkov, "An investigation of flexible waveform numerologies for 5G V2I cellular networks from a physical layer perspective," in *Proc. IEEE Int. Conf. Microw., Antennas, Commun. Electron. Syst. (COMCAS)*, Nov. 2019, pp. 1–6.

[28] L. You, Q. Liao, N. Pappas, and D. Yuan, "Resource optimization with flexible numerology and frame structure for heterogeneous services," *IEEE Commun. Lett.*, vol. 22, no. 12, pp. 2579–2582, Dec. 2018.

[29] L. Marijanovic, S. Schwarz, and M. Rupp, "Multi-user resource allocation for low latency communications based on mixed numerology," in *Proc. IEEE 90th Veh. Technol. Conf. (VTC-Fall)*, Sep. 2019, pp. 1–7.

[30] *Physical Channels and Modulation*, document TR38.211, 3GPP, 2019.

[31] L. Zhang, A. Ijaz, P. Xiao, A. Quddus, and R. Tafazolli, "Subband filtered multi-carrier systems for multi-service wireless communications," *IEEE Trans. Wireless Commun.*, vol. 16, no. 3, pp. 1893–1907, Mar. 2017.

[32] L. Zhang, A. Ijaz, P. Xiao, and R. Tafazolli, "Multi-service system: An enabler of flexible 5G air interface," *IEEE Commun. Mag.*, vol. 55, no. 10, pp. 152–159, Oct. 2017.

[33] T. Wang, J. G. Proakis, E. Masry, and J. R. Zeidler, "Performance degradation of OFDM systems due to Doppler spreading," *IEEE Trans. Wireless Commun.*, vol. 5, no. 6, pp. 1422–1432, Jun. 2006.

[34] V. D. Nguyen and H.-P. Kuchenbecker, "Intercarrier and intersymbol interference analysis of OFDM systems on time-varying channels," in *Proc. 4th IEEE Workshop Signal Process. Adv. Wireless Commun. (SPAWC)*, Jun. 2003, pp. 140–144.

[35] J. Proakis and M. Salehi, *Digital Communications*. New York, NY, USA: McGraw-Hill, 2008.

[36] A. B. Kihero, M. S. J. Solaija, A. Yazar, and H. Arslan, "Inter-numerology interference analysis for 5G and beyond," in *Proc. IEEE Globecom Workshops (GC Wkshps)*, Dec. 2018, pp. 1–6.

[37] Z.-Q. Luo and S. Zhang, "Dynamic spectrum management: Complexity and duality," *IEEE J. Sel. Topics Signal Process.*, vol. 2, no. 1, pp. 57–73, Feb. 2008.

[38] W. Dinkelbach, "On nonlinear fractional programming," *Manage. Sci.*, vol. 13, no. 7, pp. 492–498, Mar. 1967.

[39] A. Zappone, E. Björnson, L. Sanguinetti, and E. Jorswieck, "Globally optimal energy-efficient power control and receiver design in wireless networks," *IEEE Trans. Signal Process.*, vol. 65, no. 11, pp. 2844–2859, Jun. 2017.
[40] L.-H. Shen, S.-F. Hung, and K.-T. Feng, "Hybrid energy resource allocation for simultaneous wireless information and power transfer for green communications," *IEEE Trans. Green Commun. Netw.*, vol. 5, no. 4, pp. 2121–2138, Dec. 2021.
[41] W. Murray and K.-M. Ng, "An algorithm for nonlinear optimization problems with binary variables," *Comput. Optim. Appl.*, vol. 47, no. 2, pp. 257–288, 2010.
[42] E. Che, H. D. Tuan, and H. H. Nguyen, "Joint optimization of cooperative beamforming and relay assignment in multi-user wireless relay networks," *IEEE Trans. Wireless Commun.*, vol. 13, no. 10, pp. 5481–5495, Oct. 2014.
[43] L.-H. Shen, C.-Y. Su, and K.-T. Feng, "CoMP enhanced subcarrier and power allocation for multi-numerology based 5G-NR networks," *IEEE Trans. Veh. Technol.*, vol. 71, no. 5, pp. 5460–5476, May 2022.
[44] A. Khalili, S. Akhlaghi, H. Tabassum, and D. W. K. Ng, "Joint user association and resource allocation in the uplink of heterogeneous networks," *IEEE Wireless Commun. Lett.*, vol. 9, no. 6, pp. 804–808, Jun. 2020.
[45] R. Horst and N. V. Thoai, "DC programming: Overview," *J. Optim. Theory Appl.*, vol. 103, no. 1, pp. 1–43, Oct. 1999.
[46] M. Moltafet, R. Joda, N. Mokari, M. R. Sabagh, and M. Zorzi, "Joint access and fronthaul radio resource allocation in PD-NOMA-based 5G networks enabling dual connectivity and CoMP," *IEEE Trans. Commun.*, vol. 66, no. 12, pp. 6463–6477, Dec. 2018.
[47] R. Aslani, M. Rasti, and A. Khalili, "Energy efficiency maximization via joint sub-carrier assignment and power control for OFDMA full duplex networks," *IEEE Trans. Veh. Technol.*, vol. 68, no. 12, pp. 11859–11872, Oct. 2019.

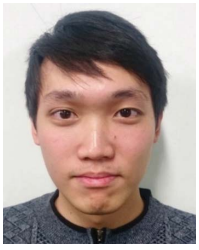

Li-Hsiang Shen (Member, IEEE) received the Ph.D. degree from the Institute of Communication Engineering, NCTU, Hsinchu, Taiwan, in 2020. Since January 2021, he has been a Post-Doctoral Researcher with the Department of Electrical and Computer Engineering (ECE), National Yang Ming Chiao Tung University (NYCU), Hsinchu. In 2018 and 2019, he was a Visiting Scholar with the Next Generation Wireless (NGW) Research Group, Electrical and Computer Engineering Department, University of Southampton, Southampton (Soton), U.K. His research interests include millimeter-wave/terahertz interference management and resource allocation, mobility-aware beam control protocol for wireless local area networks (WLANs), new radio (NR), the Internet of Things (IoT), unmanned aerial vehicle (UAV) communications, and machine/deep learning empowered wireless networks. He was awarded the first prize of the Broadcom Foundation Asia Pacific Workshop. In 2021, he was also awarded the IEEE Best Ph.D. Thesis Award, NYCU Outstanding Graduate Student—Ph.D. Research, and Phi Tau Phi Scholastic Honor Society of the Republic of China (R.O.C.).

Pei-Ying Wu received the M.S. degree from the Department of Electrical and Computer Engineering (ECE), National Chiao Tung University, Hsinchu, Taiwan, in 2021. She is currently serving as an Engineer with MediaTek Corporation. Her research interests include 5G-NR, B5G/6G, interference management, resource allocation, and numerology design.

Kai-Ten Feng (Senior Member, IEEE) received the B.S. degree from the National Taiwan University, Taipei, Taiwan, in 1992, the M.S. degree from the University of Michigan, Ann Arbor, in 1996, and the Ph.D. degree from the University of California at Berkeley, Berkeley, in 2000.

Since August 2011, he has been a Full Professor with the Department of Electrical and Computer Engineering, National Yang Ming Chiao Tung University (NYCU), Hsinchu, Taiwan, where he was an Associate Professor and an Assistant Professor, from August 2007 to July 2011 and from February 2003 to July 2007, respectively. He has been serving as the Associate Dean of the Electrical and Computer Engineering College, NYCU, since February 2017. From July 2009 to March 2010, he was a Visiting Research Fellow with the Department of Electrical and Computer Engineering, University of California at Davis. From 2000 to 2003, he was an In-Vehicle Development Manager/a Senior Technologist with OnStar Corporation, a subsidiary of General Motors Corporation, where he worked on the design of future telematics platforms and in-vehicle networks. His current research interests include broadband wireless networks, cooperative and cognitive networks, wireless indoor localization and tracking, and device-free wireless sensing technologies. He received the Best Paper Award from the Spring 2006 IEEE Vehicular Technology Conference, which ranked his paper first among the 615 accepted papers. He also received the Outstanding Youth Electrical Engineer Award in 2007 from the Chinese Institute of Electrical Engineering and the Distinguished Researcher Award from NCTU in 2008, 2010, and 2011. He has been serving as a Technical Advisor for IEEE-HKN Honor Society and the National Academy of Engineering (NAE) Grand Challenges Scholars Program (GCSP) at NCTU since 2018. He has also served technical program committees at various international conferences.